First-Spike Timing of Auditory-Nerve Fibers and Comparison With Auditory Cortex

PETER HEIL AND DEXTER R. F. IRVINE
Department of Psychology, Monash University, Clayton, Victoria 3168, Australia

Heil, Peter and Dexter R. F. Irvine. First-spike timing of auditory-nerve fibers and comparison with auditory cortex. *J. Neurophysiol.* 78: 2438–2454, 1997. The timing of the first spike of cat auditory-nerve (AN) fibers in response to onsets of characteristic frequency (CF) tone bursts was studied and compared with that of neurons in primary auditory cortex (AI), reported previously. Tones were shaped with cosine-squared rise functions, and rise time and sound pressure level were parametrically varied. Although measurement of first-spike latency of AN fibers was somewhat compromised by effects of spontaneous activity, latency was an invariant and inverse function of the maximum acceleration of peak pressure (i.e., a feature of the 2nd derivative of the stimulus envelope), as previously found in AI, rather than of tone level or rise time. Latency-acceleration functions of all AN fibers were of very similar shape, similar to that observed in AI. As in AI, latency-acceleration functions of different fibers were displaced along the latency axis, reflecting differences in minimum latency, and along the acceleration axis, reflecting differences in sensitivity to acceleration [neuronal transient sensitivity (S)]. S estimates increased with spontaneous rate (SR), but values of high-SR fibers exceeded those in AI. This suggests that S estimates are biased by SR per se, and that unbiased true S values would be less tightly correlated with response properties covarying with SR, such as firing threshold. S estimates varied with CF in a fashion similar to the cat's audiogram and, for low- and medium-SR fibers, matched those for AI neurons. Minimum latency decreased with increasing SR and CF. As in AI, the standard deviation of first-spike timing (SD) in AN was also an inverse function of maximum acceleration of peak pressure. The characteristics of the increase of SD with latency in a given AN fiber/AI neuron and across AN fibers/AI neurons revealed that the precision of first-spike timing to some stimuli can actually be higher in AI than in AN. The data suggest that the basic characteristics of the latency-acceleration functions of transient onset responses seen in cortex are generated at inner hair cell–AN fiber synapses. Implications for signal processing in the auditory system and for first-spike generation and adaptation in AN are discussed.

INTRODUCTION

Rapid temporal changes in sounds are represented in the temporal structure of the spike trains of auditory nerve fibers and central auditory neurons, as manifested in phase locking to individual cycles (i.e., to the ''fine structure'') of low-frequency sounds or to periodic changes in the envelope of amplitude-modulated sounds or in the frequency of frequency-modulated sounds (for reviews see Rhode and Greenberg 1992; Ruggero 1992; see also Cariani and Delgutte 1996). In recent years, considerable attention has been devoted to the possibility that other properties of sensory stimuli might also be coded in terms of the temporal pattern of neuronal discharges, rather than their rates (e.g., Cariani 1995; Ferster and Spruston 1995; Hopfield 1995; Middlebrooks et al. 1994). In principle, temporal coding could be provided by the temporal structure of the spike train(s) of a single neuron or by the temporal pattern across a population of neurons. The latter coding scheme would have to be favored when the responses of individual neurons consist of only a single spike or a short train of spikes in which interstimulus intervals are invariant with stimulus parameters. Onset responses, or the onset component of more complex response patterns, of neurons at many levels of the auditory pathway demonstrate such properties. For example, in auditory cortex, particularly of barbiturate-anesthetized animals, most neurons discharge only a single spike tightly locked to the onset of a stimulus (e.g., Brugge et al. 1969; Calford and Semple 1995; Evans and Whitfield 1964; Heil 1997b; Phillips 1993; for reviews see Aitkin 1990; Clarey et al. 1992), whereas the interstimulus intervals in those neurons that discharge short bursts of spikes appear to be relatively invariant with changes in basic stimulus properties (Phillips and Sark 1991; Phillips et al. 1996).

To explore possible temporal coding strategies across a population of onset neurons, knowledge of the stimulus factor(s) that might determine first-spike timing is crucial. At all levels of the auditory pathway, it is commonly observed that the first-spike latency of a given neuron decreases monotonically with the sound pressure level (SPL) of a stimulus. Because laboratory auditory signals are routinely shaped with rise times to avoid spectral splatter at signal onset, it is sometimes assumed that this decrease is due to an earlier crossing of the neuron's firing threshold during the time the signal takes to reach maximum amplitude (e.g., Kitzes et al. 1978). However, we have recently demonstrated [in primary auditory cortex (AI)], by varying SPL and rise time, that this threshold model of latency is inadequate to account for a neuron's change in latency, particularly when adaptive processes or accommodation are taken into account (Heil and Irvine 1996). In most laboratory experiments, the rise time and rise function are routinely kept constant. When SPL is varied under these conditions, the time course of the peak pressure (or envelope) during the signal's onset, as well its derivatives, such as the rate of change (1st derivative) and the acceleration of peak pressure (2nd derivative), are inevitably co-altered. Because most auditory neurons discharge spikes that are triggered by a signal's onset, it is conceivable that onset responses might be sensitive to such envelope characteristics rather than to the steady-state SPL.

In fact, we have recently identified stimulus parameters

and neuronal properties relevant for determining the timing of the first (and often only) spike of the response of neurons in AI to tone burst stimuli (Heil 1997a; Heil and Irvine 1996), as well as those relevant for determining the strength of the response (Heil 1997b). With regard to spike timing, we found, by varying SPL and rise time, that latency was an invariant function of the rate of change of peak pressure (for linear rise functions) and of the maximum (or initial) acceleration of peak pressure (for cosine-squared rise function tones), i.e., of characteristics of the derivatives of the stimulus envelope (Heil 1997a). A number of observations suggested that these characteristics of latency functions might be of peripheral origin.

The present study was undertaken to test more directly the hypothesis of a peripheral origin of the characteristics of cortical latency-acceleration functions by studying the responses of auditory nerve (AN) fibers under conditions basically identical to those used previously in the investigation of AI neurons and by directly comparing the results. Comparison of such data from auditory periphery and cortex could also provide valuable insights into the way in which first-spike timing may be shaped by the complex divergent and convergent connections within the system.

METHODS

Animal preparation

Four adult cats of either sex were prepared for recordings from the AN. All cats were free of outer and middle ear infections on the recording side (left and right for 2 cats each), as judged by otoscopic inspection. Each cat was deeply anesthetized with pentobarbitone sodium (40 mg/kg ip). Atropine sulphate (Atropin; 0.3 ml im) was administered to reduce tracheal mucous secretion. A broad-spectrum antibiotic (Amoxil; 0.5 ml im) was also given. The trachea and the radial vein were cannulated, and anesthesia was maintained throughout the experiment by intravenous injections of pentobarbitone in a physiological saline solution that also contained a few drops of heparine. The electrocardiogram was continuously monitored, and rectal temperature was held at 38 ± 0.3°C by a thermostatically controlled DC blanket. For initial surgery, the animal's head was secured in a stereotaxic frame, using blunt ear bars. A head-holder was fixed to the skull with screws and dental acrylic. A round-window electrode and a length of fine-bore polyethylene tubing, allowing static pressure equalization within the middle ear, were inserted through a small hole in the bulla on the recording side. Thereafter, the bulla was resealed with dental acrylic, the external meatus was cleared of surrounding tissue, transected to leave only a short meatal stub, and the ear bar was removed. Also on the recording side, the skull was trephined caudal to the tentorium, the dura was removed, and the cerebellum over the cochlear nucleus was aspirated. The auditory nerve was then exposed near its exit from the internal auditory meatus by gently pushing and holding the cochlear nucleus medially with small saline-soaked cotton swabs.

Acoustic stimulation and recording procedures

The cat was located in a sound-attenuating chamber. Stimuli were digitally produced (Tucker Davis Technology) and presented to the cat's ear via a calibrated sealed sound delivery system, consisting of a STAX SRS-MK3 transducer in a coupler (Sokolich 1981). The calibration procedure has been described in detail elsewhere (Heil et al. 1992a). The sound delivery tube of the coupler fitted snugly into the meatal stub. The compound action-potential audiogram was examined in response to 10-ms tone bursts with 1-ms linear rise times. The activity of single AN fibers was recorded with micropipettes, filled with a solution of pontamine sky blue in 3 M KCl or NaCl, and with impedances of ~7–10 MΩ at 1 kHz. Under visual control through an operating microscope, the micropipette was positioned manually on the surface of the nerve, using a dorsoposterior to ventroanterior and a slightly medial-to-lateral approach. The pipette was further advanced by means of a remote-controlled stepper-motor microdrive. Neural activity was amplified (1,000 times), filtered (500–5,000 Hz), passed through a Schmitt-trigger, and displayed on storage oscilloscopes. The discriminator level was unaltered during data acquisition when it was possible to do so without losing the fiber. Event times were stored on disk with 10-μs resolution for off-line analysis.

Once a fiber was isolated, its characteristic frequency (CF; frequency of lowest response threshold) was determined by manually varying the stimulus frequency and amplitude. Quantitative data were obtained with CF tone bursts that were presented under computer control. All tone bursts were of 200-ms total duration and were shaped with symmetrical cosine-squared rise and fall functions. At tone onset the peak pressure (PP; in Pa), i.e., the tone burst envelope, changes as a function of time t (in s) according to

$$PP = PP_{plateau} * \cos^2 (t/CRT * \pi/2 + \pi/2) \quad \text{with} \quad 0 \le t \le CRT \quad (1)$$

where CRT is the cosine-squared rise time (in s) and $PP_{plateau}$ the plateau peak pressure.

The rate of change of peak pressure (RCPP; in Pa/s), i.e., the first derivative of the envelope, varies with time according to

$$RCPP = -\pi/CRT * PP_{plateau} * \cos (t/CRT * \pi/2 + \pi/2) * \sin (t/CRT * \pi/2 + \pi/2) \quad (2)$$

RCPP is maximal halfway through the rise time and is given by

$$RCPP_{max} = PP_{plateau}/2 * \pi/CRT \quad (3)$$

The acceleration of peak pressure (APP; in Pa/s^2), i.e., the second derivative of the envelope, varies with time according to

$$\begin{aligned} APP &= -(\pi/CRT)^2/2 * PP_{plateau} * [\cos^2 (t/CRT * \pi/2 + \pi/2) \\ &\quad - \sin^2 (t/CRT * \pi/2 + \pi/2)] \\ &= -(\pi/CRT)^2/2 * PP_{plateau} * \cos (2\pi * t/CRT + \pi) \end{aligned} \quad (4)$$

Maximum APP occurs at the beginning of the rise time and is given by

$$APP_{max} = PP_{plateau}/2 * (\pi/CRT)^2 \quad (5)$$

The time courses of peak pressure, rate of change, and acceleration of peak pressure for cosine-squared rise functions are schematically illustrated in Fig. 1. It should be emphasized that the envelope of a signal is a construct (for a detailed account of the notion of an envelope, see Viemeister and Plack 1993). A tone burst's envelope becomes more and more elusive as the period of the carrier frequency increases and accounts for an increasingly significant fraction of the rise time. This gradually fading envelope construct also has a counterpart in the generator potential of inner hair cells (IHCs) in response to tones. At high frequencies, the envelope of the signal is more or less closely reflected in the time course of the DC component of the generator potential. With decreasing frequency the DC component decreases, whereas the AC component, which reflects the signal's fine structure, increases (see Palmer and Russell 1986; Russell and Sellick 1983).

Twenty or 50 repetitions of CF tones with a given rise time were presented at 2 Hz, at SPLs ranging from below threshold up to 90 dB SPL (re 20 μPa) in 10-dB steps. This was followed by recording the spikes in the same number of repetitions of 210-ms

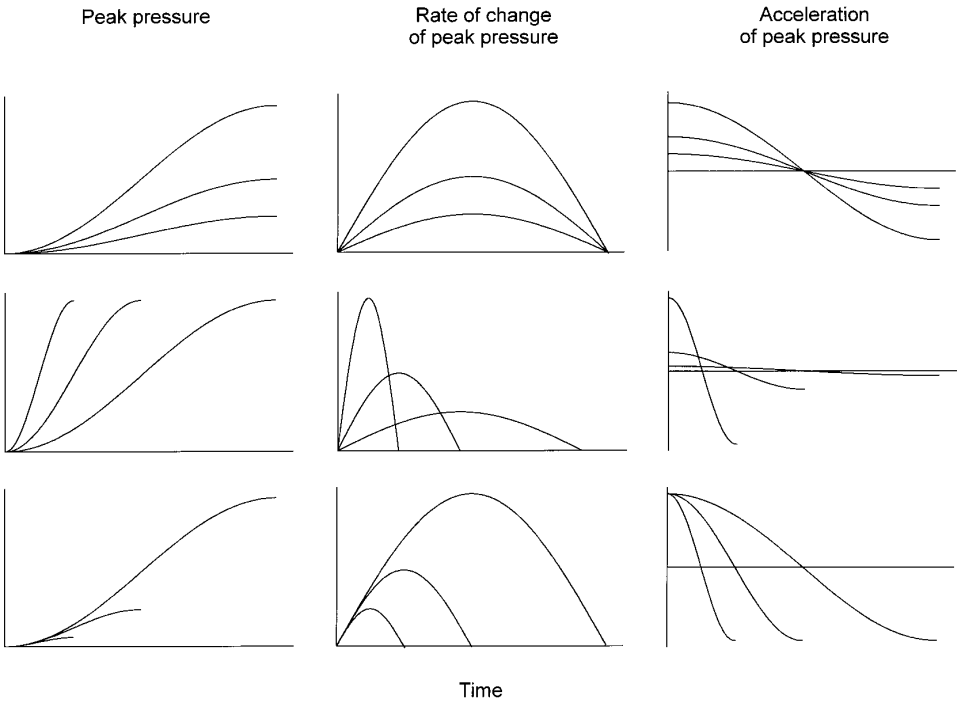

FIG. 1. Envelope characteristics of the onsets of tone bursts shaped with cosine-squared rise functions. Panels in the *left column* show, for 3 different stimuli, the time courses of peak pressure during the rise time. Only the top halves of the symmetrical envelopes are illustrated. The *middle* and *right columns* show the resulting time courses of the rate of change of peak pressure and of the acceleration of peak pressure, respectively. Signals in the *top row* have identical rise time, but differ in plateau peak pressure, rate of change, and acceleration of peak pressure. Signals in the *middle row* have identical plateau peak pressure, but differ in rise time, rate of change, and acceleration of peak pressure. Signals in the *bottom row* have identical maximum acceleration of peak pressure, but differ in plateau peak pressure, rise time, and rate of change of peak pressure.

time windows, also at 2 Hz, during which no stimulus was presented. These no-stimulus windows were used to derive measures of spontaneous activity (see below). A different rise time was then selected and the recording procedure repeated. As many as six different rise times, covering the range of 1.7–85 ms, were tested and presented in random sequence. Note that tones of the same SPL but different rise time have different total energy.

Data analysis

Spikes in response to the 20 or 50 presentations of a given stimulus were displayed off-line as a poststimulus time histogram. The total number of spikes in a 210-ms window commencing with tone onset and summed over all repetitions was the measure of response for a tone of a given SPL and rise time. Firing threshold was defined as the lowest level of a tone that elicited more spikes than the mean number of spikes plus two standard deviations (SDs) recorded in the no-stimulus intervals. For each combination of SPL and rise time, the latency of the first spike on each repetition of that stimulus within the 210-ms window was used to calculate the mean and SD of the latency. Latency measures were not corrected for acoustic delays of ~0.25 ms.

RESULTS

Database

A total of 77 AN fibers were studied. Two cats provided the bulk of the data (*95-107*: $n = 25$ and *96-001*: $n = 42$), whereas the other two cats served mainly for a different project and provided only limited data to the present study. The fibers had CFs ranging from 0.6 to 35.5 kHz. Spontaneous discharge rate (SR) varied from zero or near-zero to ~90 spikes/s. According to the classification of Liberman (1978), 10 fibers (13%) were low-SR ($\leq$0.5 spikes/s), 27 (35%) were medium-SR ($>0.5 \leq 18$ spikes/s), and 40 (52%) were high-SR ($>$18 spikes/s).

First-spike latency of auditory nerve fibers and implications of spontaneous activity

FIRST-SPIKE LATENCY VERSUS RESPONSE LATENCY. Before we present data on the first-spike latencies of AN fibers, some consideration of the effects of spontaneous activity on latency measurements is required. When a fiber is spontaneously active, the first spike that occurs after stimulus onset is not necessarily a spike that was evoked by that stimulus. Thus mean *first-spike* latency may not accurately reflect the fiber's true *response* latency. However, because there is no a priori knowledge of which spike in a spike train following the onset of a stimulus is the first evoked by the stimulus, the problem of determining the response latency, as distinguished from the first-spike latency, cannot be overcome simply by delaying the analysis window relative to stimulus onset. The likelihood of the first spike being spontaneous, rather than evoked by the stimulus, obviously increases with the fiber's SR and with the latency of the first stimulus-evoked spike. Thus, when a fiber *responds* on every trial, but is also spontaneously active, mean first-spike latency can be shorter than the true response latency. However, when the fiber's response probability is less than one, i.e., near threshold, diverse effects may be anticipated. Consider the case where a fiber responds only to some of the repetitions of a near-threshold stimulus and does so with some particular latency. During the other repetitions the fiber is only spontaneously active. Then, the mean first-spike latency based on all repetitions could be longer or shorter than the response latency, depending on the response probability, on the response latency, and on SR. Mean first-spike latency could be longer than the response latency (termed here a ''negative near-threshold effect''), when the response probability is low, the actual response latency short, and the SR low or medium. With this conjunction of characteristics, the stan-

dard deviation (SD) of first-spike latency might also be larger than that of the response latency. Mean first-spike latency could be shorter than the response latency (''positive near-threshold effect'') when the SR is high and the response latency long. Finally, it must be kept in mind that, because of the refractory period following a spike, spontaneous activity might also delay somewhat the occurrence of the first truly evoked spike. To obtain an estimate of the influence of spontaneous activity on mean first-spike latency, the mean ± SD of the first-spike in 20 or 50 no-stimulus windows was calculated. This sample of spontaneous activity was obtained following the last presentation of a 90-dB SPL tone with a given rise time.

FIRST-SPIKE LATENCY. Figure 2*B* plots mean first-spike latency as a function of tone level (in dB SPL) and rise time for a medium-SR fiber. For each rise time, mean first-spike latency decreases monotonically with tone level, and at high tone levels the latency functions obtained with different rise times appear to converge on a single minimum. The range over which latency decreases with level is more restricted for short rise times, and, for tones of most given levels, latency increases monotonically with rise time, although at levels below 30 dB SPL the increase is rather irregular.

In Fig. 2*C* the same data are plotted as a function of the maximum acceleration of peak pressure. To a large extent, the six latency functions obtained with the different rise times are in close register. Only the data points from each function obtained with tones of the two or three lowest SPLs deviate from the common course taken by the other points, in that mean latencies to those stimuli are mostly much longer than those to the other stimuli with the same acceleration. A comparison with the neuron's spike count functions (Fig. 2*A*) shows that tones of 10 and 20 dB SPL do not evoke activity much above the neuron's SR (horizontal dashed line), whereas tones of ≥30 dB are clearly suprathreshold. These deviant means were therefore likely caused by near-threshold effects, as outlined above. Furthermore, the deviant mean latencies obtained from this fiber to 10- and 20-dB SPL tones, and for 85-ms rise time also to 30-dB SPL tones, all fall in the range of, or even exceed, mean first spike latencies that result from spontaneous activity (''mean spontaneous latencies''; diamonds near ordinate in Fig. 2*C*). Furthermore, the variability of the first-spike recorded to low-SPL tones was as high as that of spontaneous activity. This is shown in Fig. 2*D*, which plots the SD of first-spike latency against maximum acceleration of peak pressure. SDs of the first-spike latency of spontaneous activity ranged from ~35 to 65 ms (diamonds near ordinate in Fig. 2*D*), a range also obtained with low-SPL tones. Thus the mean first-spike latencies to stimuli near threshold, i.e., with levels of 10 and 20 dB SPL, appear to be dominated by spontaneous activity rather than by evoked spikes. When these values are disregarded, the fiber's mean first-spike latency is an unambiguous function of the maximum acceleration of peak pressure, as was recently reported for AI neurons (Heil 1997a), irrespective of the stimulus level or rise time. The improvement in the match of latency functions when plotted as a function of acceleration rather than of SPL is considerable, even for the shorter rise times, commonly used in physiological studies, and for high SPLs. This is evident from a comparison of Fig. 2*E* and Fig. 2*F*, which replot the data of Fig. 2*B* and Fig. 2*C*, respectively, with a higher resolution of the ordinate.

Equivalent data from a high-SR fiber are presented in Fig. 3. Again, latency functions obtained with tones of different rise time are in much closer register when plotted as a function of maximum acceleration of peak pressure (Fig. 3*C*) than of SPL (Fig. 3*B*), even for short rise times and high SPLs (compare Fig. 3, *F* and *E*). Also, the means and SDs of measured latencies to some low-SPL tones were in the range of, or even exceeded, measures based on the fiber's spontaneous activity [viz., 9–20 ms for latency (Fig. 3*C*); 6–18 ms for SD (Fig. 3*D*)]. When the common course of the latency-acceleration function formed by the high-SPL tones is visually extrapolated toward lower values of acceleration, the mean latencies to the low-SPL tones (10–40 dB) of 85-ms rise time appear to fall below this function, i.e., latencies are shorter than expected on the basis of the magnitude of acceleration. This positive near-threshold effect is to be expected from the high SR in combination with a rather long response latency. In contrast, mean latencies to some low-SPL tones of short rise times (e.g., 10 dB SPL with 1.7- to 8.5-ms rise time, cf. Fig. 3, *A* and *B*) are longer than expected on the basis of the magnitude of acceleration, a negative near-threshold effect that might be explained by a shorter response latency and a low response probability, as reasoned above.

However, the fact that negative near-threshold effects were also seen in fibers with very low SRs makes it unlikely that the above interpretations hold generally. Data from two such fibers are illustrated in Figs. 4 and 5. Only mean first-spike latencies to tones louder than ~20 dB above threshold are in close register, when plotted as a function of maximum acceleration of peak pressure, whereas mean latencies to the low-SPL tones are all considerably longer than the latencies to the higher-SPL tones of the same acceleration (Figs. 4*C* and 5*C*). Although the response probabilities to some of these low-SPL stimuli were low, the latency mismatch could hardly have been caused entirely by the very rare spontaneous spikes. The average total number of spikes recorded in the 20 no-stimulus trials was 0.5 for *fiber 96-001/13* and 1.0 for *fiber 96-001/42*, values too low to be indicated by dashed lines in Figs. 4*A* and 5*A*, as was done in Figs. 2 and 3. The variability of the timing of the first spike to the low-SPL tones is also quite high (Figs. 4*D* and 5*D*), reflecting the fact that at these SPLs the first spike of these fibers, although likely evoked by the stimulus, could basically occur at any instant during the stimulus duration. In other words, the first spike in these fibers and at these levels is neither a spontaneous one, nor one that is precisely locked to the stimulus onset.

Shape of latency—acceleration functions of AN fibers and comparison with AI

To assess the shapes of latency-acceleration functions of AN fibers and to compare them with those of AI neurons, which have negligible SRs (e.g., Fig. 7*A*) and discharge mostly onset responses, latency-acceleration functions of

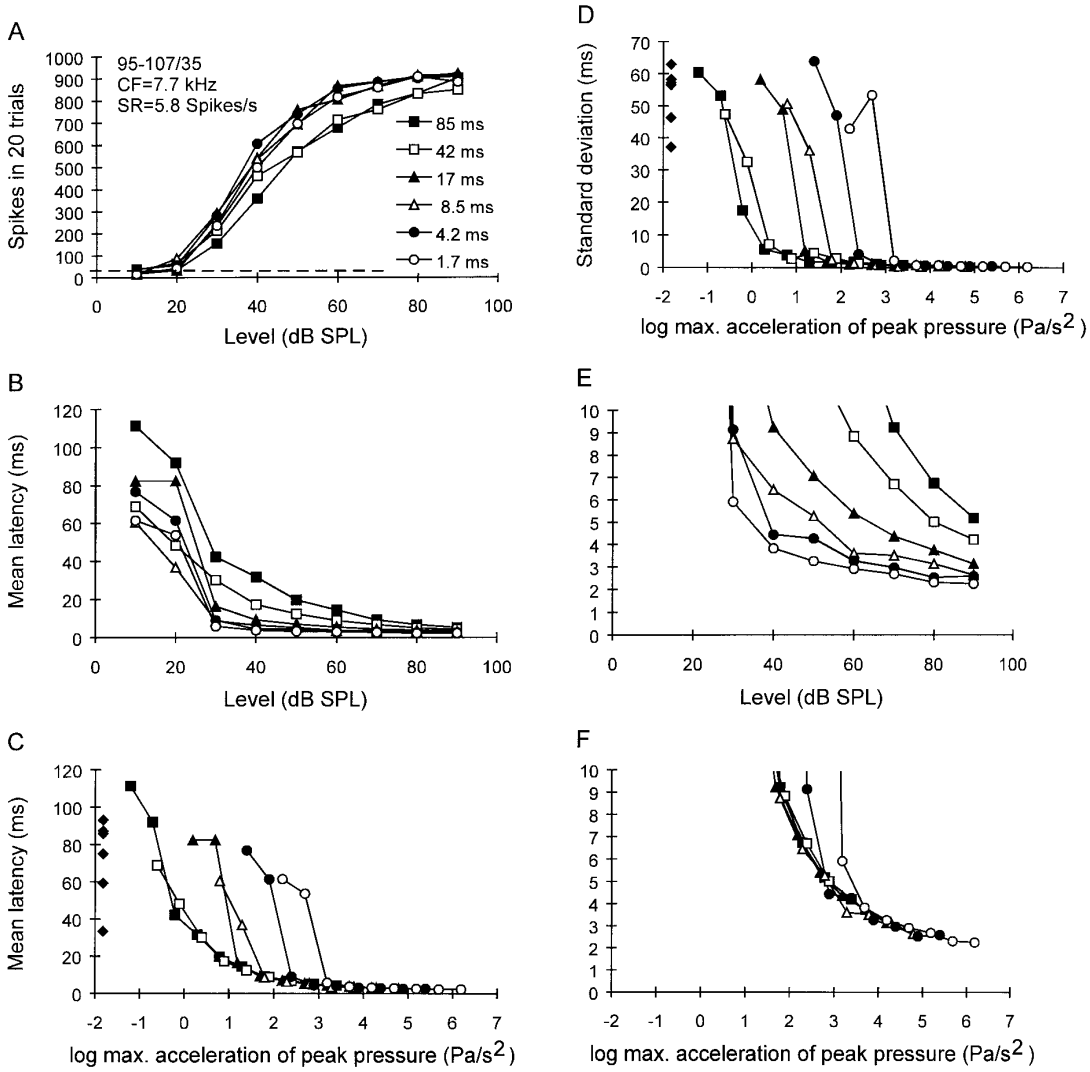

FIG. 2. Tone response measures of a medium spontaneous rate (SR) fiber (*95-107/35*). *A*: total number of spikes to 20 repetitions of characteristic frequency (CF; 7.7 kHz) tones of 200-ms duration recorded in a 210-ms window commencing with tone onset as a function of tone level (in dB SPL) and rise time (different symbols). The legend, which provides the key to the symbols, applies to all panels. The dashed horizontal line indicates the mean number of spikes recorded in the 6 $\times$ 20 no-stimulus windows of 210-ms duration each, viz., 24.3 spikes, yielding a SR of 5.8 spikes/s. *B*: mean first-spike latency obtained with tones of different rise times plotted as a function of level. *C*: mean latency plotted as a function of the logarithm of maximum acceleration of peak pressure (measured in Pa/s^2). The 6 diamonds near the ordinate represent the ''mean spontaneous latencies'' obtained from the 6 $\times$ 20 no-stimulus windows. *D*: standard deviation of first-spike latency plotted as function of the logarithm of maximum acceleration of peak pressure. The 6 diamonds near the ordinate represent the ''spontaneous standard deviations'' obtained from the 6 $\times$ 20 no-stimulus windows. *E* and *F*: same data as in *B* and *C*, respectively, plotted with higher resolution of the ordinate.

AN fibers were curtailed to reduce the influence of near-threshold effects, described above, on the shape of the function. For high-SR and medium-SR fibers, this was done by discarding means of first-spike latency for which either the mean or the corresponding SD or both exceeded the lowest mean latency or SD obtained for spontaneous activity. For *fiber 95-107/35* (Fig. 2), for example, application of these criteria meant that mean latencies to all 10- and 20-dB tones, and for 85-ms rise time also to 30-dB tones, were discarded. For *fiber 95-107/34* (Fig. 3), mean latencies to tones up to and including 40 dB SPL for 85- and 42-ms rise times, 20-dB SPL for the 17-ms rise time, and 10-dB SPL for the three shortest rise times were discarded. For low-SR fibers, for which the ''spontaneous latency'' criteria were inappropriate, mean latencies obtained within $<$20 dB of firing threshold were discarded. Thus, for the low-SR *fibers 96-001/13* and *96-001/42* (Figs. 4 and 5), mean latencies to all tones $\leq$40 dB SPL were discarded.

Figure 6*A* (symbols) shows such curtailed latency-acceleration data from another five fibers with CFs ranging from 4.2 to 35.2 kHz. All fibers have medium SR so that each function can be followed to relatively long latencies at low values of maximum acceleration of peak pressure. It is apparent that the latency-acceleration functions of the five fibers are of very similar shape. In fact, this was true for the entire sample. The functions differ with respect to their position

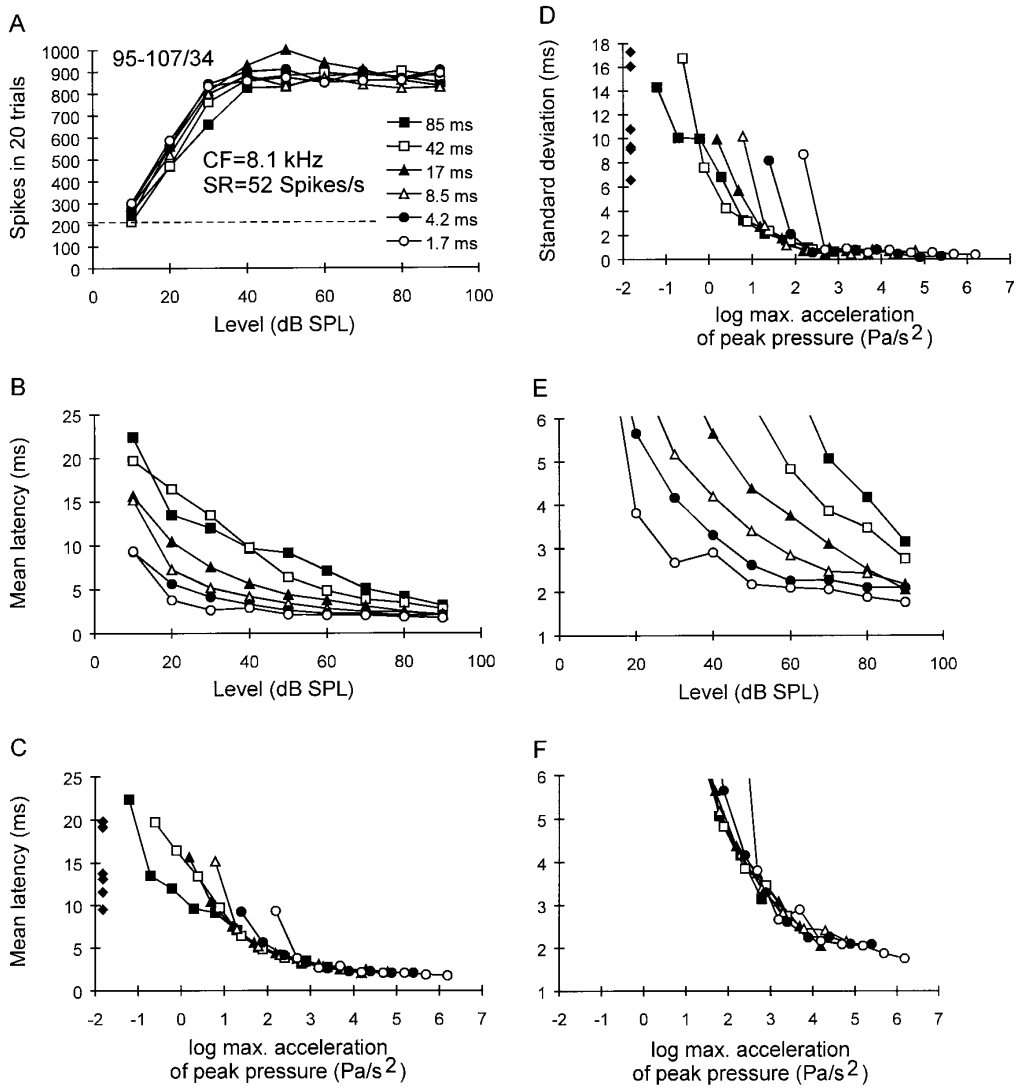

FIG. 3. *A–D*: tone response measures of a high-SR fiber (*95-107/34*). Conventions as in Fig. 2.

within the coordinate system, i.e., they differ somewhat in the minimum value against which latencies asymptotically converge at high values of acceleration of peak pressure, and, more conspicuously, they are dispersed along the abscissa.

Equivalent observations were made previously on latency-acceleration functions of AI neurons (Heil 1997a). For comparison, five such functions from AI neurons, also covering a wide CF range, are illustrated in Fig. 6*B*. When latency-acceleration functions of AN fibers are compared with those of AI neurons, it is apparent that functions from those two auditory structures are also of similar shape (cf. Fig. 6, *A* and *B*). We have therefore decided to use the same type of formula to describe mathematically the latency-acceleration functions of AN fibers as that used previously for functions of AI neurons (Heil 1997a)

$$L = L_{\min} + A/(\log \mathrm{APP}_{\max} + S)^4 \qquad (6)$$

where L is a fiber's mean first-spike latency as a function of the maximum acceleration of peak pressure $\mathrm{APP}_{\max}$. $\mathrm{APP}_{\max}$ is a function of both tone level and rise time (*Eq. 5*). $L_{\min}$ is the minimum or asymptotic latency against which L converges with $\mathrm{APP}_{\max}$ approaching infinity. It is thought to include all those delays that are independent of the magnitude of the stimulus, such as acoustic delays, middle-ear conduction time, traveling wave delays, the axonal travel time to the recording site, and the minimum synaptic delay at the IHC–afferent fiber synapse. S denotes a neuronal sensitivity to acceleration of peak pressure, more generally termed ''transient sensitivity'' (Heil 1997a), and is given in log units of $\mathrm{APP}_{\max}$ in $\mathrm{Pa/s^2}$. A large S value represents a high transient sensitivity and indicates a latency-acceleration function in a relatively leftward position within the coordinate system (e.g., *96-001/08* in Fig. 6*A*) and vice versa. The difference in S values for two fibers directly identifies the displacement of their latency-acceleration functions along the abscissa. A is a scaling factor.

The best fit of *Eq. 6* to the actual data from a given fiber was found by an iterative procedure that minimized the sum of the squared deviations, each weighted with the fiber's response probability, between the data and *Eq. 6* (Heil

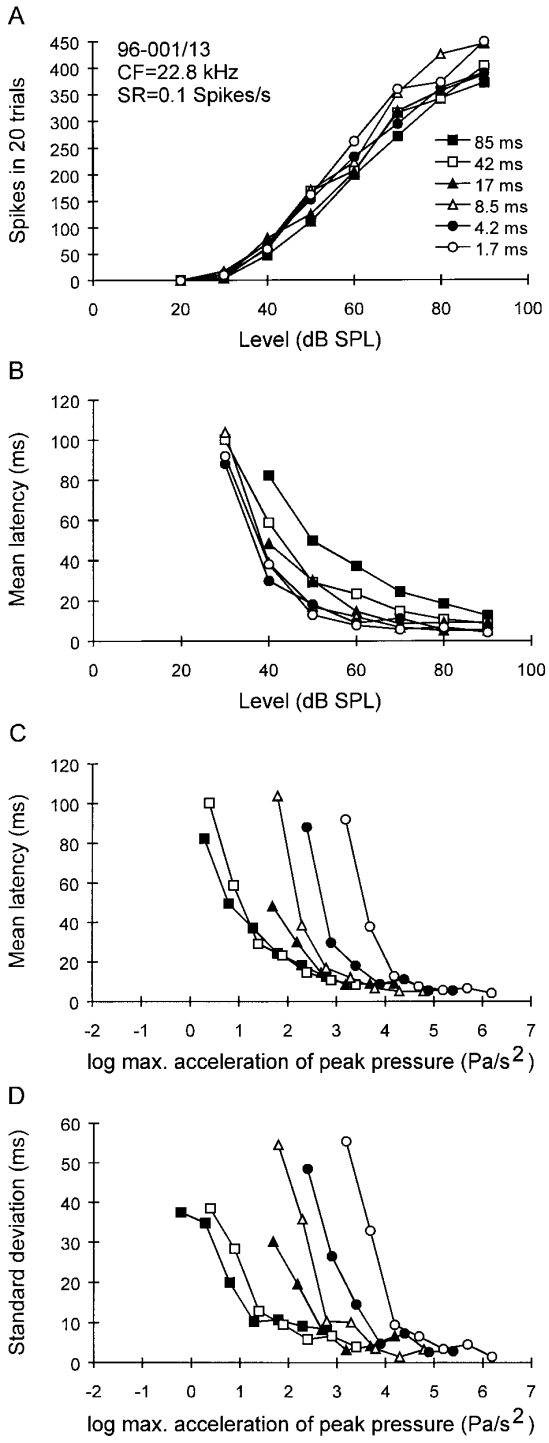

FIG. 4. *A–D*: tone response measures of a low-SR fiber (95-001/13). Conventions as in Fig. 2, except that higher-resolution panels are not provided.

1997a). In the first fitting step, L_{min}, S, and A were free parameters. The scaling factor A showed a unimodal distribution across the fiber population with a mean of 13.3 s, very close to the equivalent value for the population of AI neurons (viz., 12.8 s). In a second and final fitting step, A was held fixed at 13.3 s. In so doing, a function with a fixed form was fitted to the data from each fiber. The estimates obtained for S and L_{min} from this second fitting step then specified the latency-acceleration function's position along the abscissa and ordinate, respectively.

For each of the five fibers for which the measured latency-acceleration data are shown by symbols in Fig. 6*A*, the best fit of *Eq. 6* with $A = 13.3$ s is also illustrated (solid and dashed lines). Note that the best fits closely approximate

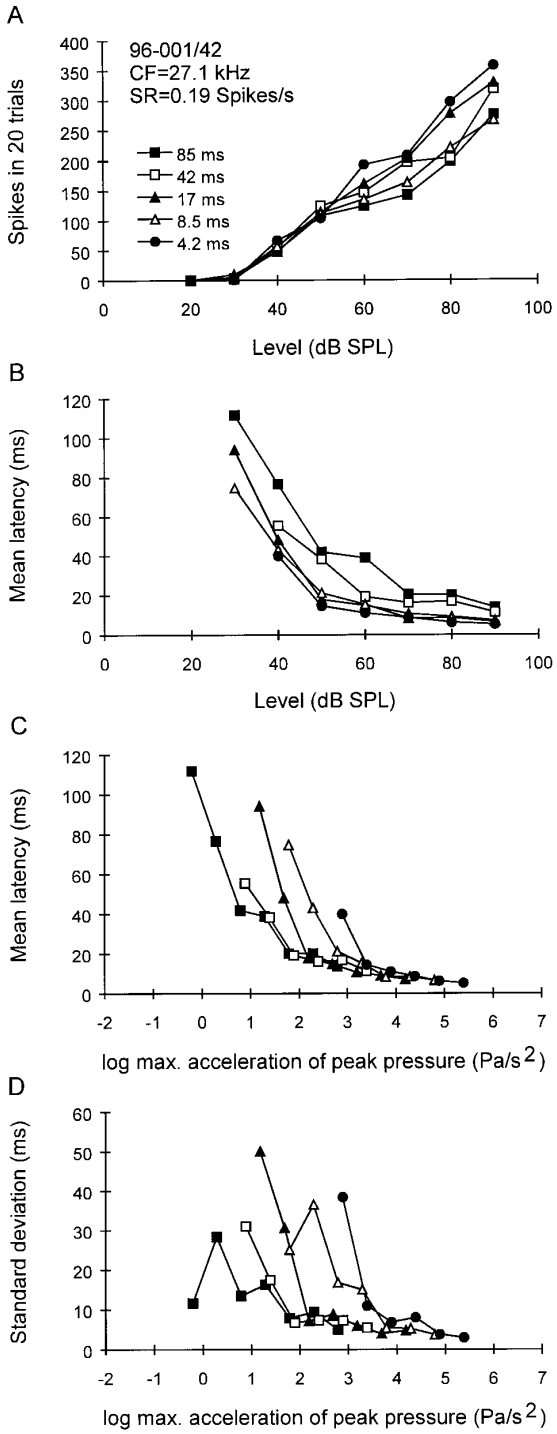

FIG. 5. *A–D*: tone response measures of a low-SR fiber (96-001/42). Conventions as in Fig. 4.

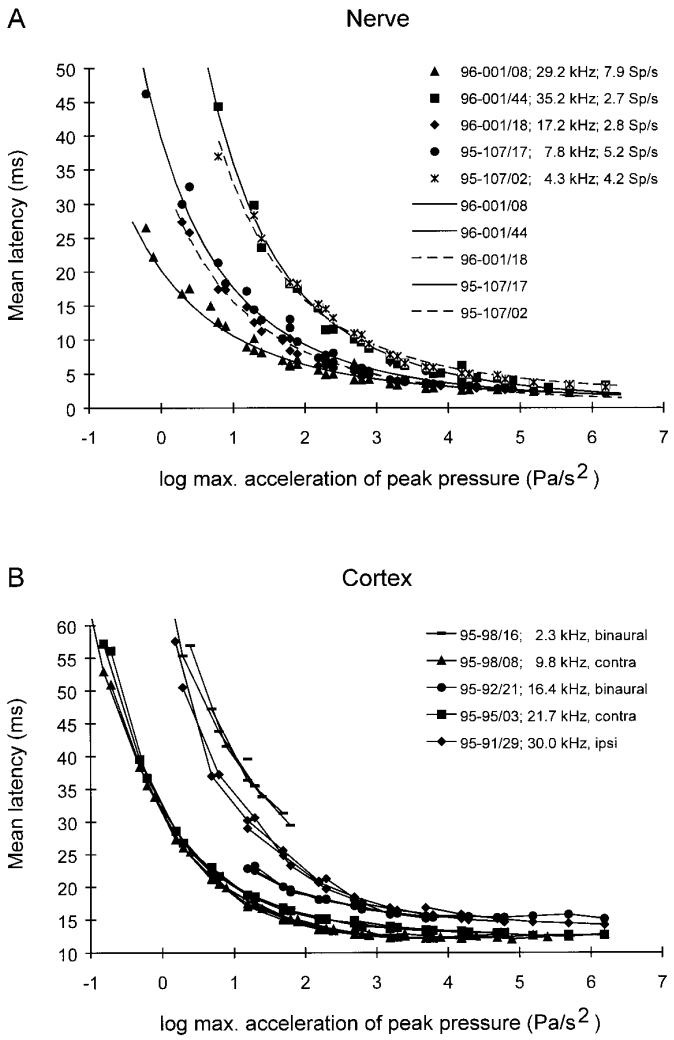

FIG. 6. Comparison of latency-acceleration functions of auditory nerve (AN) fibers (*A*) and primary auditory cortex (AI) neurons (*B*). Data from fibers/neurons from different cats and with different CFs were selected to illustrate the similarity in the shapes of the latency-acceleration functions despite differences in extent. Cortical data were also obtained with different laterality of stimulus presentation. In *A* and *B*, mean latencies obtained from a given fiber/neuron are represented by the same symbol, and in *B*, latencies obtained from a given neuron with tones of the same rise time are also connected by continuous lines. In *A*, the best fits of *Eq. 6* with $A = 13.3$ s to the data for each fiber are shown by continuous and dashed lines (see legend). Note the good match of the fitted functions with the data. For further descriptions see RESULTS.

the measured data, thus *Eq. 6* with $A = 13.3$ s provides a rather accurate description of the actual change of first-spike latency with maximum acceleration of peak pressure.

Some interdependencies of parameters of latency—acceleration functions and comparison with auditory cortex

TRANSIENT SENSITIVITY AND SPONTANEOUS RATE. A fundamental correlation established for AN fibers is that between SR and firing threshold (e.g., Kiang et al. 1965; Kim and Molnar 1979; Liberman 1978; Rhode and Smith 1986; Winter et al. 1990), a relationship also found in our sample ($r = 0.439$; $n = 76$; $P < 0.001$; with logarithm of SR). It is therefore of interest to determine whether a similar relationship may exist between SR and the measure of transient sensitivity derived from the latency-acceleration functions. Note that firing threshold (measured in Pa or dB SPL) and transient sensitivity (measured in Pa/s^2) are different measures. Figure 7A provides a scatterplot of S estimates against SR. For SRs above ~2 spikes/s, the S estimates increase systematically with SR, and the correlation ($r = 0.758$; $n = 77$; $P < 0.001$; with logarithm of SR) is stronger than that for firing threshold and SR. However, in judging the relative strengths of these correlations, it has to be kept in mind that, although latency-acceleration functions were curtailed to eliminate near-threshold effects, spontaneous activity still results in mean first-spike latencies that are shorter than the corresponding true response latencies, and therefore results in S estimates that are somewhat higher than the values that would be derived from true response latencies, if these true S values were available. Because the S estimates, compared with the true S values, will be biased in a SR-dependent fashion, the correlation between SR and S estimates is likely to be somewhat stronger than that between SR and true S

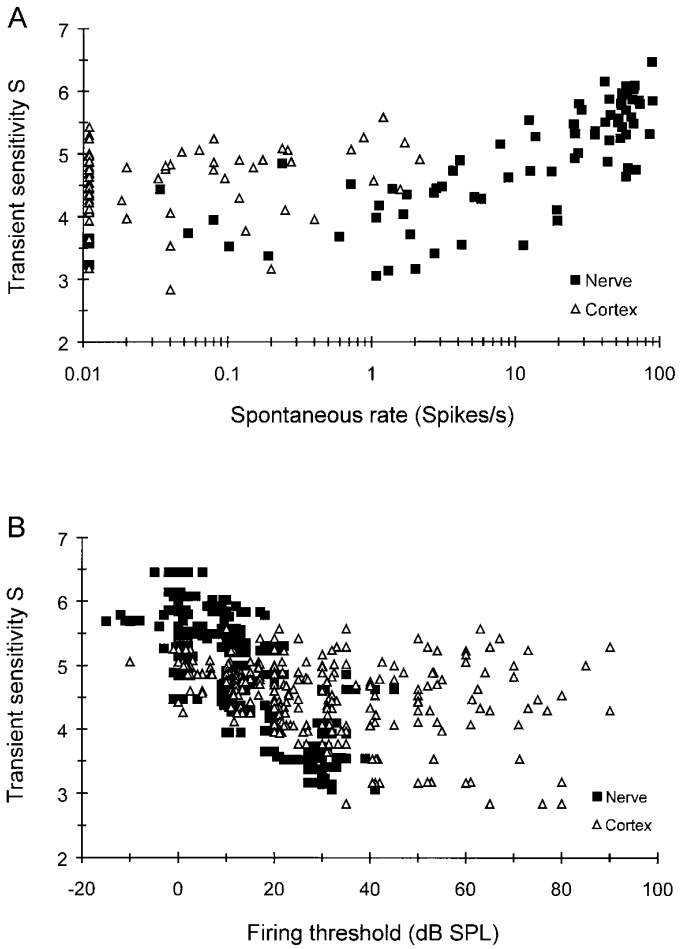

FIG. 7. Scatterplots of the estimate of transient sensitivity against spontaneous discharge rate (*A*) and firing threshold as defined in RESULTS (*B*). Solid squares and open triangles represent data from AN and AI, respectively. To enable the inclusion of fibers and neurons without spontaneous activity in *A*, they were assigned a SR of 0.011 spikes/s.

values, but how much stronger is difficult to quantify. In AI, where SRs are low, S estimates and SR are uncorrelated ($r = 0.198$; $n = 75$; $P > 0.05$; Fig. 7*A*).

TRANSIENT SENSITIVITY AND FIRING THRESHOLD. Because of the correlations of SR with firing threshold and with transient sensitivity, threshold and S estimate are also expected to be correlated. Figure 7*B* shows a scatterplot of the two measures. Each fiber provided multiple data points to the figure as a firing threshold was assigned for each rise time tested, although in the AN rise time has little, if any, effect on the firing threshold (e.g., Fig. 2*A* to 5*A*). A linear regression analysis between firing threshold (x) and S estimate (y) revealed a slope of -0.057 with $r = 0.759$ ($n = 333$). For comparison, data from the auditory cortex are also shown in Fig. 7*B* (open triangles). In cortex, where the neuronal discharges are phasic in contrast to the predominantly tonic response of AN fibers, the SPL of a tone required to elicit a threshold response (threshold criterion was a response probability of 0.1) generally increased with the rise time of the tone (Heil 1997b). This leads to a considerable spread of the data points along the abscissa of Fig. 7*B*, and, compared with the nerve data, to a shallower slope (viz., -0.009) and a smaller correlation coefficient (viz., $r = 0.351$ with $n = 319$). Yet, when only the lowest threshold, i.e., that to tones with the shortest rise time tested, is taken into account, the slope and the correlation coefficient for the cortical data increase somewhat (viz., -0.027 with $r = 0.606$ and $n = 70$), but are still less than those for the nerve, which are basically unaltered by this selection procedure (viz., -0.060 with $r = 0.734$ and $n = 76$). As the S estimates are biased relative to those of true S values, the slope and the strength of the correlation between true S values and firing threshold in AN might be more similar to those in AI.

TRANSIENT SENSITIVITY AND CHARACTERISTIC FREQUENCY. In Fig. 8*A*, S estimates are plotted as a function of characteristic frequency, separately for low-, medium-, and high-SR fibers. Note that the ordinate is reversed. S estimates are highest in the CF range from around 10–20 kHz, and fall off toward lower and higher frequencies, with the fall-off toward higher CFs being much steeper. This distribution resembles that for AI (open triangles), but the range of S estimates at any given CF is much wider in AN than in AI. At any CF, the S estimates of most high-SR fibers are not reached by the cortical neurons. The distribution of AI points matches more closely those of medium- and low-SR fibers, an observation more clearly illustrated in Fig. 8*B*, which plots the mean of the S estimates in 1–3 kHz wide CF bands (see Fig. 8 legend) as a function of CF, separately for high- and for medium/low-SR fibers, and for AI neurons. Note that the shapes of the three functions are similar, but that for high-SR fibers is shifted by about one unit of S. This result again suggests that, because S estimates of AN fibers are biased due to spontaneous activity, true S values might show a distribution more similar to that seen in AI. Nevertheless, it is also possible that there are intrinsic differences between fibers of different SR that also lead to different S values.

RELATIONSHIPS OF MINIMUM LATENCY. The minimum latency L_{min}, as estimated from the fit of *Eq. 6* to the latency-acceleration functions, was closely correlated with ($r = 0.952$ with $n = 77$), and on average 1.3 ms shorter than, the shortest mean latency recorded. The difference is expected given that even for short rise-time tones of high SPL the fibers had not reached their asymptotic values (see, e.g., Figs. 2, *E* and *F*, and 3, *E* and *F*).

There is a significant negative relationship ($r = -0.423$; $n = 77$; $P < 0.001$) between L_{min} and the log of SR, and long minimum latencies prevail in the low-SR range (not shown). Finally, there is a general trend for L_{min} to decrease with increasing CF (Fig. 9; solid squares). In the CF range around 20 kHz, a fiber with extremely long minimum latency of ~22 ms, possibly an efferent fiber, and a cluster of six fibers with minimum latencies of 4–6 ms, much longer than those of other fibers in the corresponding CF range, stand out. At 1.6 kHz there is another such fiber. These long estimates of minimum latency are not artifacts of the fitting procedure, because the shortest mean latencies of these fibers were in a similar range. The spike count level functions of five of these fibers were nearly straight, whereas three had sloping-saturation characteristics. SRs were mostly very low,

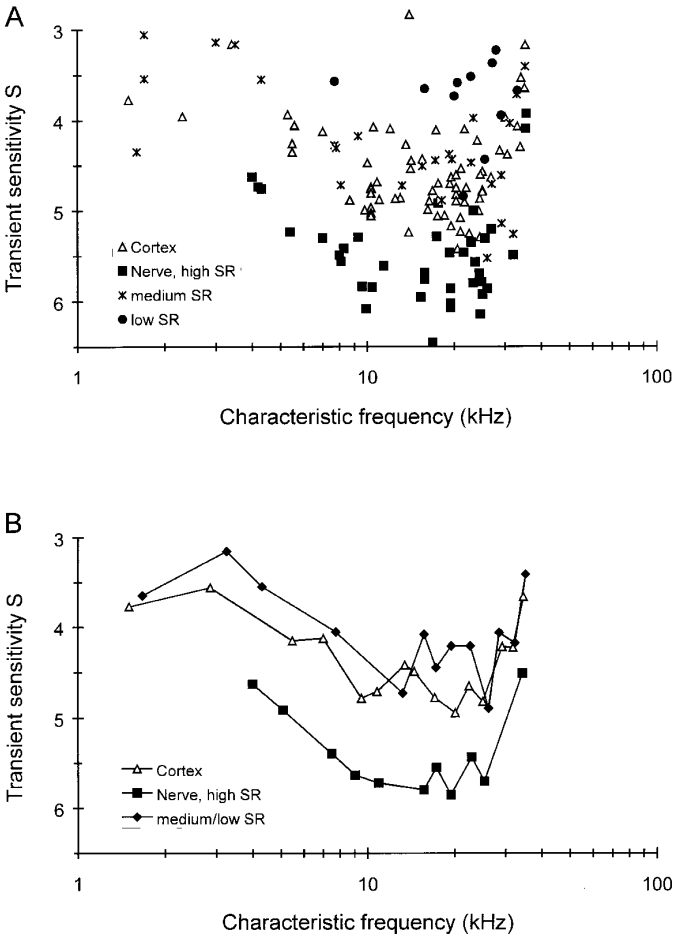

FIG. 8. *A*: scatterplot of the estimates of transient sensitivity against characteristic frequency, separately for low-SR, medium-SR, and high-SR fibers, and for AI neurons. *B*: means of S estimates of high-SR and medium/low-SR fibers and of AI neurons with CFs within restricted CF bands plotted against CF. Upper limits of the CF bands: 2, 4, 6, 8, 10, 12, 14, 16, 18, 21, 24, 27, 30, 33, and 36 kHz. Note that in *A* and *B* the ordinates are reversed.

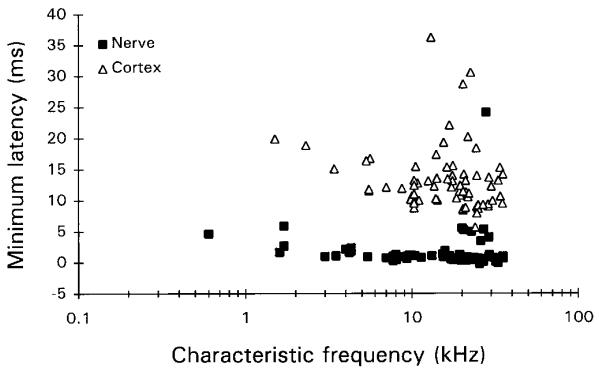

FIG. 9. Estimated minimum latency of AN fibers and AI neurons plotted as a function of CF.

except for two fibers that belonged to the medium-SR group and had sloping-saturation level functions. The two fibers illustrated in Figs. 4 and 5 are among these long-latency fibers.

Figure 9 also provides a comparison of the CF dependence of $L_{\min}$ of AN fibers and AI neurons. Minimum latencies in AI (open triangles) are, of course, considerably longer than those of AN fibers, and with the exception of the possible efferent, there is virtually no overlap between the two populations. The distribution of $L_{\min}$ at a given CF is wider in AI than in AN. The data, although somewhat sparse, also suggest that the decline of the shortest minimum latencies with CF may be more pronounced in AI than in AN.

Standard deviation of first-spike latency

In cortex, it was observed that the SD of first-spike latency is also a function of maximum acceleration of peak pressure, rather than of rise time or of tone level (Heil 1997a). The shape of an AI neuron's SD-acceleration function was distinctly different from the shape of the corresponding latency-acceleration function, arguing against a linear relationship between SD and latency. Rather, the nature of the shape differences suggested that SD was proportional to the slope of the latency-acceleration function. Such a relationship could be brought about, or be closely approximated by, jitter in the term ($\log \mathrm{APP}_{\max} + \mathrm{S}$) of *Eq. 6*, i.e., jitter in the acceleration of peak pressure or in the neuron's transient sensitivity. As a result, SD would increase with latency in a nonlinear, rather than in a linear, fashion (Heil 1997a).

Figures 2*D* to 5*D* illustrate that SD of AN fibers is also a function of maximum acceleration of peak pressure, when, as was done with latency, near-threshold data are discarded. Data on the growth of SD with latency from four fibers are presented in Fig. 10. As outlined above, if the SD-acceleration function were a scaled version of the latency-acceleration function, then SD would increase linearly with latency

$$\mathrm{SD} = \mathrm{SD}_{(0)} + k_{\mathrm{Lin}} * L \qquad (7)$$

where k_{Lin} is the slope of the increase and $\mathrm{SD}_{(0)}$ the hypothetical standard deviation for $L = 0$. The minimum standard deviation $\mathrm{SD}_{\min}$ is obtained for $L = L_{\min}$.

If SD were proportional to the slope of the latency-acceleration function, viz. if

$$\mathrm{SD} = \mathrm{SD}_{\min} + k * \dot{L} \qquad (8)$$

where SD converges against $\mathrm{SD}_{\min}$ when the slope $\dot{L}$ of the latency-acceleration function approaches zero at high values of acceleration of peak pressure, and k is the proportionality factor, then SD should increase nonlinearly with L: with $\dot{L}$, the first derivative of *Eq. 6*, given by

$$\dot{L} = -4A * (\log \mathrm{APP}_{\max} + \mathrm{S})^{-5}$$

it follows that SD grows with latency according to

$$\mathrm{SD} = \mathrm{SD}_{\min} - 4k * (1/A)^{1/4} * (L - L_{\min})^{5/4} \qquad (9)$$

Equations 7 and *9* were both fitted to the data for each fiber. Only SD values corresponding to those mean latencies that had been used in the fits of latency data were included. The linear model (*Eq. 7*) described the data well with an average r^2 of 0.855 (range 0.443–0.987). However, it provided a better fit to the data in only 40% (31/77) of cases, whereas the nonlinear model (*Eq. 9*) did so in 60% of cases (46/77), as well as across the entire sample. The best linear and nonlinear fits of the data for the four fibers in Fig. 10 are illustrated by dashed and continuous lines, respectively. Thus, as in AI, SD of first-spike latency of AN fibers appears to be somewhat better decribed as being proportional to the slope of the latency-acceleration function rather than to latency itself.

COMPARISON OF PRECISION OF FIRST-SPIKE TIMING IN AUDITORY NERVE AND CORTEX. In Fig. 11, the coefficient k is plotted against SR (solid squares). There is strong negative correlation between k and SR or its logarithm ($r = -0.858$ and $r = -0.737$, respectively; $n = 76$). In other words, and because a larger negative k value represents a steeper increase of SD with latency, the higher SR the steeper is that increase. This trend is also clearly visible in the four data sets illustrated in Fig. 10.

When the distribution of k in the nerve is compared with that obtained in the cortex (Fig. 11, open triangles), it is evident that the distribution in cortex is much narrower, and that for most AI neurons k is relatively small, i.e., for AI neurons compared with AN fibers the increase in SD with latency is rather shallow. Even when the comparison is restricted to the fibers and neurons with a similar range of SRs (i.e., below 2.5 spikes/s), k is smaller for AI neurons (mean of 0.12) than for AN fibers (mean of 0.28).

Figure 12 provides a scatterplot of the smallest SD measured against the shortest latency measured from AN fibers (solid symbols), both on logarithmic axes, with data from low-, medium-, and high-SR fibers identified by different symbols. Note that the log of minimum SD increases roughly linearly with the log of minimum latency. A linear regression analysis between the *logarithms* of the two measures yielded a slope of 1.67 ± 0.12 (mean $\pm$ SE) and an ordinate intercept of -1.04 ± 0.05 (top solid line in Fig. 12) with $r = 0.844$; $n = 77$. Thus the growth of minimum SD with minimum latency in the AN is well described by the power function

$$\mathrm{SD}_{\min} = 0.09 \times (L_{\min})^{1.67} \qquad (10)$$

Also note that low-SR and high-SR fibers tend to prevail at opposite ends of the elongated data cloud. In other words, low-SR fibers tend to have longer minimum latencies (as

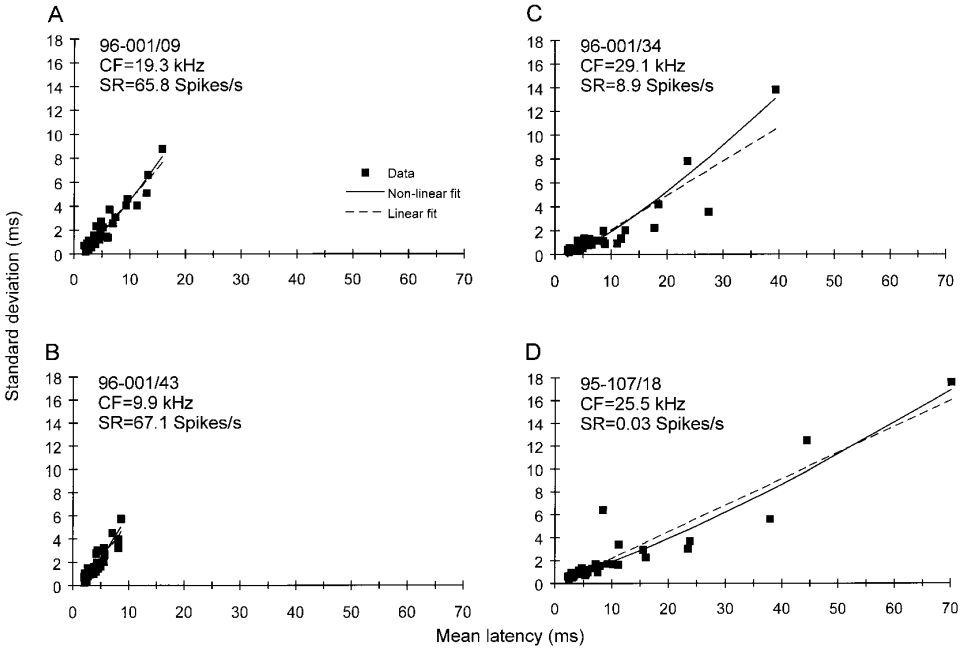

FIG. 10. *A–D*: plots of SD vs. mean latency for 4 AN fibers, differing in CF and SR. Note that SD increases more rapidly with mean latency for high-SR fibers and least rapidly for low-SR fibers. Dashed and solid lines represent the best fit of *Eqs. 7* and *9*, respectively. These assume that SD is proportional to mean latency (*Eq. 7*) or to the slope of the mean latency-acceleration function (*Eq. 9*).

established above) and a larger minimum variability of first-spike timing than high-SR fibers.

Figure 12 also allows a comparison of AN data with corresponding data obtained from AI neurons (open triangles). For AI neurons, latency and SD represent the mean latency and corresponding mean SD to the three CF tone bursts most effective in driving the neuron. For monotonic neurons these were short-rise time, high-SPL tones, whereas for nonmonotonic neurons these could be medium-SPL tones. As for AN, there is a linear relationship between the *logarithms* of the two measures with a slope of 2.09 ± 0.13 and a y-intercept of -2.61 ± 0.16 (bottom solid line in Fig. 12) with $r = 0.830$, $n = 115$. Thus the growth of minimum SD with minimum latency for AI neurons is well described by the power function

$$SD_{min} = 0.0025 \times (L_{min})^{2.09} \quad (11)$$

The power function for AI is shifted almost parallel to that for AN, as reflected in similar exponents but markedly different coefficients in *Eqs. 10* and *11*.

Figure 12 also illustrates that, although there is hardly any overlap of the distributions of minimum latency of AN fibers and AI neurons, there is considerable overlap in the distributions of their minimum first-spike variabilities, although larger minimum SDs are more common in AI than in AN. This is more clearly illustrated in Fig. 13, which plots the minimum SDs in AN (solid triangles) and AI (open triangles) as cumulative percentage functions. The shallower slope and rightward displacement of the function for AI relative to that for AN reflects the higher incidence of larger minimum SDs in AI compared with AN.

However, the rates of growth of SD with mean latency are generally higher for AN fibers than for AI neurons (Fig. 11), so that for stimuli for which latency and corresponding SD are some distance away from their respective minimum

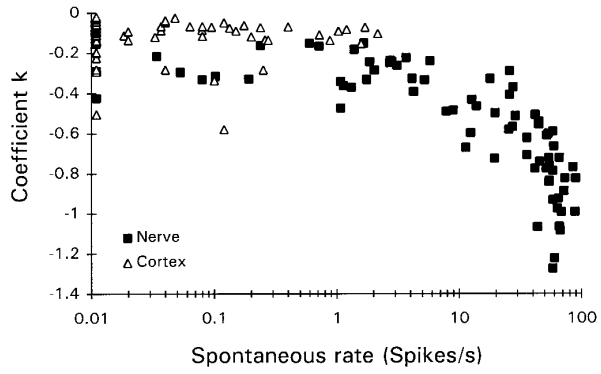

FIG. 11. Plot of the coefficient k of *Eq. 9* vs. spontaneous discharge rate for AN fibers and AI neurons. Note that in the nerve the magnitude of k increases with SR and that, for similar SRs, values are larger in AN than in AI.

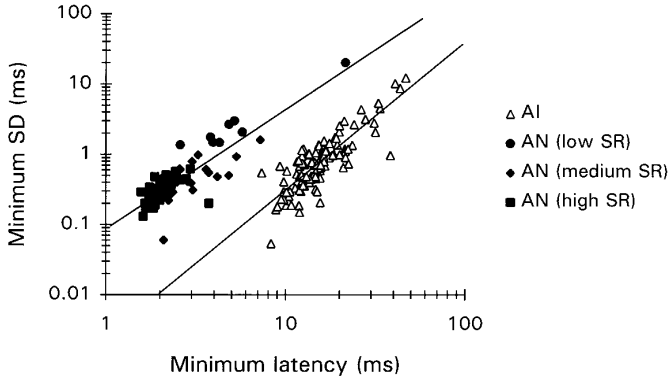

FIG. 12. Scatterplots of measured near-minimum standard deviation vs. corresponding near-minimum latency for AN fibers (solid symbols) and AI neurons (open triangles). AN fibers are further distinguished by SR. The oblique solid lines represent the power functions fitted to the AN and AI data (*Eqs. 10* and *11*). See RESULTS for further description.

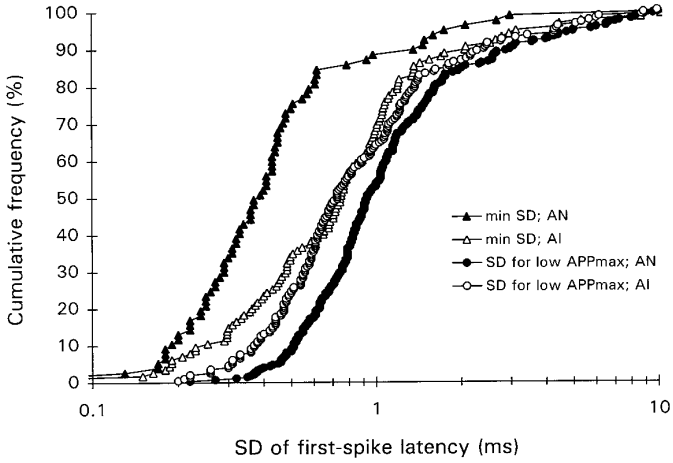

FIG. 13. Cumulative percentage functions of SD in AN and AI. Solid and open triangles represent the minimum SD of AN fibers and AI neurons, respectively (same data as in Fig. 12). Solid and open circles represent SDs of AN fibers and AI neurons (those tested with CF tones of cosine-squared rise functions; $n = 65$) (data from Heil 1997a) measured in response to the same set of tones. Tones had different rise times and SPLs, viz. 85 ms/90 dB SPL; 42 ms/80 dB SPL; 17 ms/60 dB SPL; 8.5 ms/50 dB SPL; 4.2 ms/40 dB SPL and 1.7 ms/20 dB SPL, but were of similar, relatively low, maximum acceleration of peak pressure (logarithms of 2.69–2.89). Consequently, these tones evoked responses with very similar mean latency and SD from a given fiber or neuron. To avoid near-threshold effects, only tones with SPLs at least 20 dB above firing threshold were considered; the inclusion of near-threshold data would have displaced the AN function even further to the right of the AI function.

values, the distributions of SDs in AN and AI may be more similar. Figure 13 illustrates that for stimuli of similar, relatively low maximum acceleration of peak pressure (logarithms of 2.69–2.89; compare with Figs. 2–6) the SD distribution for AN (solid circles) is shifted to the right of that for AI (open circles), indicating that first-spike latency for such stimuli is more precise in AI than in AN.

DISCUSSION

The present study has demonstrated that the first-spike latency of AN fibers to CF tones shaped with cosine-squared rise functions is an invariant function of the maximum acceleration of peak pressure, as was previously shown to be the case for AI neurons (Heil 1997a), rather than of SPL or rise time. Furthermore, the shape of latency-acceleration functions across AN fibers was very similar and was also similar to that observed in AI. As in AI, latency-acceleration functions were displaced along the latency axis, reflecting differences in minimum latency, and along the acceleration axis, reflecting differences in sensitivity to acceleration (transient sensitivity). The variability of first-spike timing (SD) in AN was also a function of maximum acceleration of peak pressure. The increase of SD with mean latency is somewhat better described by a nonlinear than by a linear relationship, as was the case in cortex. These data support our previous conclusion that characteristics of the latency-acceleration function reflect processes at the synapses between IHCs and AN fibers.

Comparison of basic findings in auditory nerve with previous studies

Minimum latency increased with decreasing SR (Fig. 12), a finding in agreement with results of Rhode and Smith (1986), who demonstrated that, at any given CF, high-SR fibers had the shortest and low-SR fibers the longest latencies. Because the unmyelinated peripheral terminal of high-SR fibers tends to be of larger caliber than that of low-SR fibers (Liberman 1982; Merchan-Perez and Liberman 1996), it is likely that differences in associated passive membrane properties contribute to the latency differences, but differences in synaptic features, such as size or shape of synaptic bodies (Liberman 1980; Merchan-Perez and Liberman 1996), may be involved as well. SR was also found to correlate with firing threshold, and fibers with high and medium SRs were of saturating (Fig. 3*A*) or sloping/saturating (Fig. 2*A*) nature, whereas the functions of fibers with long minimum latencies and low SRs tended to have straight spike count–level functions (e.g., Figs. 4 and 5), largely in agreement with previous studies (e.g., Kim and Molnar 1979; Liberman 1978; Rhode and Smith 1986; Sachs and Abbas 1974; Winter et al. 1990). However, to our knowledge, straight level functions for CF tones have not previously been described in the cat. The four straight functions recorded in the present study were from fibers with CFs between 20 and 28 kHz and were recorded in the cat that yielded the largest number of fibers. We cannot entirely exclude the possibility that we may have misjudged CF, although CF determination in these fibers is particularly straightforward given their low SRs. There may have been an undetected slight hearing loss in that frequency region in that cat, although the firing thresholds of none of the other 16 fibers with CFs in a 19- to 28-kHz range, nor any of the remaining 22 fibers with CFs outside this range, provided evidence for such a loss. Straight level functions and low SRs are also characteristic features of efferent fibers of the medial olivocochlear system (see Liberman 1988; Liberman and Brown 1986), so that it may be argued that some recordings may have been from efferent rather than afferent fibers. However, the minimum latencies of high-CF (>2 kHz) efferents recorded by Liberman and Brown (1986) were all longer than ~15 ms (with the exception of one binaurally driven efferent), considerably longer than the minimum latencies recorded in the present study. Only *96-001/29* with a CF of 27.9 kHz may have been an efferent fiber. Its minimum latency was ~24 ms, and its maximum average firing rate was by far the lowest of all fibers studied (112 spikes in 4.2 s, i.e., ~27 spikes/s, compared with ~100 spikes/s for other low-SR fibers with straight level functions, see Figs. 4 and 5; and up to ~250 spikes/s in fibers of medium and high SRs, Figs. 2 and 3).

Minimum latency also decreased with CF (Fig. 9), in a manner qualitatively similar to that observed by Rhode and Smith (1986) and similar to the decrease of group delays measured in squirrel monkey (Anderson et al. 1971), cat (Goldstein et al. 1971; Joris and Yin 1992), guinea pig (Palmer and Russell 1986), and chinchilla (Ruggero and Rich 1987). The asymptotic value reached at high CFs by our estimates of L_{min}, which were derived from the fits, was somewhat shorter than the values of 1–2 ms reported in the studies cited above, a discrepancy that obviously results from the different methodologies.

The measure of transient sensitivity, which describes the relative displacement of latency functions along the accelera-

tion axis, has not been applied previously to AN fibers. It was found here that S estimates were correlated with SR (Fig. 7*A*), so that, at any given CF, high-SR and low-SR fibers had the highest and lowest S estimates, respectively (Fig. 8). We have argued here that the estimate of S, which was derived from analysis of the first-spike latency, as distinguished from the true response latency, was affected by the spontaneous activity of the fiber, so that S estimates can be higher than the corresponding true S values; the more so the higher SR. It follows then that the slope and the strength of the correlation between S estimates and SR overestimate the slope and the strength of the correlation between the corresponding true S values and SR. It cannot be ruled out that true S values and SR may even be uncorrelated, as is the case in AI, where SRs are low and S estimates are therefore equivalent to true S values. With these effects of SR on S estimates in mind, it is noteworthy that, at any given CF, S estimates of medium/low-SR fibers matched those of AI neurons, which have low SRs, whereas those of high-SR fibers were higher than the highest estimates obtained in AI (Fig. 8). Although it could be argued that high-SR fibers simply lack a representation in AI, this is extremely unlikely, as for example, firing thresholds (in dB SPL) of AI neurons (e.g., Heil et al. 1992b, 1994; Phillips 1990; Schreiner et al. 1992) are as low as those of high-SR AN fibers (e.g., Liberman 1978). The inevitable bias produced by SR on S estimates also has the consequence that for AN the slope and strength of the correlation between S estimate and firing threshold, which is correlated with SR (e.g., Kiang et al. 1965; Kim and Molnar 1979; Liberman 1978; Rhode and Smith 1986; Winter et al. 1990), overestimates the slope and strength of the correlation between true S values and threshold. This conclusion is supported by the observed differences in the slopes and strengths of the correlations between transient sensitivity and firing threshold in AN and AI. It needs to be reemphasized that, although the two measures are correlated and S estimates vary with CF in a manner grossly similar to the cat's audiogram measured under similar experimental conditions (Rajan et al. 1991), transient sensitivity and firing threshold are different measures.

Comparison of first-spike timing in auditory nerve and cortex

LATENCY. Although the first-spike latency of AN fibers is compromised as a measure of response latency by spontaneous activity, it showed dependencies on stimulus parameters strikingly similar to those of first-spike latency in AI. At both levels of the auditory pathway, first-spike latency was an unambiguous function of the maximum acceleration of peak pressure, and not of SPL or rise time. Furthermore, the shapes of latency-acceleration functions of AN fibers and AI neurons are remarkably similar (Fig. 6). This was emphasized by the emergence of a similar average scaling factor (viz., 13.3 s for AN and 12.8 s for AI) when the same type of power function with identical sign and magnitude of power was used to fit the latency functions. Also, the neuronal transient sensitivities derived from these fits were related to CF by functions whose shapes were similar for AN and AI (Fig. 8). When the comparison was restricted to populations with similar SR, the match even applied to the values obtained (Fig. 8*B*). Thus when the effects of SR on this measure (see DISCUSSION above) are taken into account, the relative CF-dependent displacements of latency functions along the acceleration axis are likely very similar in AN and AI.

Minimum latencies in AI were considerably longer than those in AN, basically without overlap of the populations (Figs. 9 and 12). The longer latencies in AI are, of course, expected, given the longer pathways and the higher number of serial synapses over which AI neurons receive their inputs. However, the distribution of minimum latency over CF for AI is not simply a delayed version of that for AN. Rather, there is a larger scatter of minimum latencies at a given CF in AI than in AN, and the decline of minimum latencies with CF appears to be steeper. The greater scatter of minimum latencies presumably reflects the fact that input to AI is conveyed over multiple parallel brain stem and forebrain pathways (e.g., Clarey et al. 1992; Irvine 1992 for reviews). A steeper decline of (near-minimum) latencies with CF than expected from cochlear delays was also observed in the inferior colliculus of cat (Langner et al. 1987) and gerbil (Heil et al. 1995), and in the auditory cortex analogue of the domestic chick (Heil and Scheich 1991). Within the latter structure, the decline was shallowest for the input layer, and steepest for the layer highest up the processing hierarchy. The significance of these findings is as yet unclear, but it is noteworthy that the above studies provided direct or indirect evidence for a correlation of latency with preferred modulation frequency of amplitude-modulated signals.

PRECISION OF FIRST-SPIKE TIMING. The present study has also demonstrated that minimum SD grows with minimum latency, and that for both AN and AI these relationships are best described by power functions (*Eqs. 10* and *11;* Fig. 12). In their study of the posterior field (P) of the cat's auditory cortex, Phillips et al. (1995) have also provided a scatterplot of minimum SD versus latency, both on logarithmic axis, of AI (and field P) neurons. As judged by eye, their measurements from AI neurons (see their Fig. 9) are in excellent agreement with those of the present study.

As evident from the existence of a power relationship between SD and latency for AN, this relationship originates from pre- and postsynaptic factors across only a single synapse. The SDs of AI neurons are much smaller than those obtained by extrapolation to longer latencies of the trend seen in the AN data (Fig. 12), and as reflected in a smaller coefficient of the power function. On the other hand, the distribution of SDs of AI neurons is not simply a delayed version of that seen in AN (note that in Fig. 12 latency is plotted on a logarithmic axis). Two different antagonistic processes may be expected to operate in the central auditory system whose joint effects may underlie the differences in the power function of AI compared with that of AN. On the one hand, the variability of first-spike timing in the afferent axon(s) would be expected to be multiplied by some factor in the postsynaptic neuron, so that minimum SD would increase with increasing number of synapses and hence with increasing minimum delay along the pathway. Those spherical bushy cells of the anteroventral cochlear nucleus

(AVCN) that receive input from only one AN fiber via a ''secure'' end-bulb-of-Held–type synapse might be well suited to study this effect. On the other hand, additional cellular mechanisms, such as the requirement of coincident inputs for spike generation, might counteract this effect. For example, Joris et al. (1994) have shown that the phase locking of fibers of the trapezoid body, which originate from bushy cells in the AVCN, to low-frequency CF tones is more precise than that of AN fibers. They developed a model that generated such improved synchronization and assumed convergence of multiple AN fibers onto a bushy cell and a spike-generating mechanism in that cell that required coincidence of input spikes. Also, there is ample evidence that cortical neurons function as coincidence detectors (for review see König et al. 1996).

Although there was hardly any overlap of the distributions of minimum latency for AN fibers and AI neurons (Fig. 12), the corresponding distributions of minimum SDs spanned a similar range, a finding also made by Phillips (1993) on the basis of a comparison of data sampled in different laboratories (Phillips and Hall 1990; Rhode and Smith 1986). Nevertheless, AI has a higher proportion of large SDs (Figs. 12 and 13), so that on average the maximal precision of first-spike timing is higher in AN than in AI. However, this comparison refers only to those tone burst stimuli that, in a given neuron, evoke a response with near-minimum latency and near-minimum SD. For any given neuron, SD grows (nonlinearly) with latency, and does so at faster rates for AN fibers than for AI neurons (Fig. 11). Consequently and perhaps surprisingly, first-spike timing to some stimuli can, on average, be even more precise in AI than in AN (Fig. 13).

Some implications for signal processing in the auditory system

The similarities of the behavior of first-spike timing in AN and AI demonstrated here suggest that this behavior is likely to be shared by the onset responses of neurons at all levels between AN and AI, and possibly beyond AI. If this were the case, then the responses to CF tones of a particular rise function (here: cosine-squared) of all AN fibers and onset neurons in the central auditory system would exhibit latency functions of basically identical shape. Neurons/fibers differ with respect to the extent of their functions, due to differences in threshold and, for central neurons, in nonmonotonicity of responses (Fig. 6*B*) (see also Heil 1997b). Neurons/fibers also differ with respect to minimum latency and transient sensitivity, both in a CF-dependent fashion (Figs. 8 and 9). The shape of the latency function itself is likely to depend on, and vary with, the shape of the tone burst's rise function. For example, it was found in AI that the shape of latency-acceleration functions, recorded to tones of cosine-squared rise functions, differed from that of latency versus rate of change of peak pressure functions, recorded to tones of linear rise functions (Heil 1997a). For a given neuron, the transient sensitivity is also a function of tone frequency, but these transient sensitivity–frequency functions differ for different neurons (Heil 1997a). Major differences among neurons and at different levels of the auditory neuraxis are therefore expected with respect to the displacement of latency functions along the latency axis for off-CF frequencies (see Fig. 6 in Heil 1997a).

For AI neurons it was shown that the latency function also has an important consequence for the magnitude of their onset responses (Heil 1997b). The probability or the number of spikes of an AI neuron's response to tone burst onsets is a function of the instantaneous peak pressure (envelope) at the time of response generation and not of the steady-state SPL (Heil 1997b). The time of response generation is given by the difference between the response latency and the minimum latency. The response latency is a function of maximum acceleration of peak pressure, and the peak pressure at the instant of response generation depends on the time course of the envelope. Thus, and as explained and illustrated in more detail elsewhere (Heil 1997b), a neuron's onset response represents a sample of the envelope taken at a particular instant. The numerical value of that sample could be represented, for example, by the ratio of the responses of neurons with the same transient sensitivity to that stimulus, i.e., of neurons that generate their responses at the same instant, but have different and overlapping response versus instantaneous peak pressure functions. Samples of the changing envelope at different instances are taken by neurons that generate their responses at different times after stimulus onset, i.e., that differ with respect to their transient sensitivity to that stimulus (Heil 1997b). With regard to a tone burst onset, the population of neurons sampling the envelope in this way would include neurons with different CFs, because a neuron's transient sensitivity is a function of frequency. In this way the changing envelope could be tracked and represented by the onset responses of different neurons. Because latency-acceleration functions of different neurons have the same shape (Fig. 6), the temporal sequence of response generation to stimuli of different acceleration (e.g., stimuli that differ in SPL and/or in rise time) will be the same. Importantly, and because latency-acceleration functions approach each other with increasing acceleration, the intervals between the times of response generation of different neurons are shorter for stimuli of high acceleration than for those of low acceleration. In other words, the sampling rate is adjusted to the rapidity of the envelope changes. Of course, this proposed tracking relies on the orderly temporal sequence of response generation in that responsive population of neurons. Consequently, the representation of fine stimulus details would be limited by the precision of spike timing relative to the sampling rate. Because the SD of first-spike latency decreases with latency (Fig. 10) (see also Heil 1997a), the precision is high when the time of response generation is short and vice versa. This stimulus dependence of SD counteracts an increase in the temporal overlap of response initiation among the successively activated neurons that will occur with an increase in the rapidity of the transient. Thus the temporal resolving capacity of this system, which would be much higher than might be inferred from the ability of AI neurons to phase lock to repetitive stimuli, such as amplitude-modulated tones (e.g., Eggermont 1991; Schreiner and Urbas 1988), would be largely unaffected by the overall SPL of a given stimulus.

The data of the present study support the view that a similar tracking mechanism, as outlined above for AI and originally proposed by Heil (1997b), might operate among onset responses of neurons at all levels of the auditory pathway. Such a tracking mechanism is clearly not restricted to tone burst onsets but could function for a range of envelope transients, including formant transitions.

Implications with respect to first-spike generation and adaptation in auditory nerve

The previous finding in AI that the magnitude of a neuron's onset response (i.e., the number of spikes per stimulus) is a function of the instantaneous peak pressure at the time of first-spike generation, given by the difference between the response latency and the minimum latency (i.e., by $L - L_{\min}$), is equivalent to stating that the response is a function of the integral of rate of change of peak pressure over a window whose duration is given by $(L - L_{\min})$ and which commences with the stimulus (Heil 1997b). For cosine-squared rise function tones, the latency in turn is a function of APP_{max} (and hence of rise time and SPL; see *Eq. 5*). As this latency behavior was also demonstrated here for AN fibers, the similarity suggests that the magnitude of the initial response of an AN fiber, i.e., the number of spikes that are locked to the tone's onset, may be determined by a similar mechanism as the magnitude of the onset response of AI neurons, i.e., by integration of the rate of change of peak pressure within a window given by $(L - L_{\min})$. If this were the case, then the onset response of AN fibers would be expected to behave differently than the steady-state discharge, determined by the steady-state SPL. Several studies have indeed reported that the initial sharp onset peak seen in the peristimulus time histograms of most AN fibers behaves rather independently from the steady-state discharge rate. For example, the peak-to-steady-state ratio increases with stimulus amplitude (Kiang et al. 1965; Rhode and Smith 1986; Westerman and Smith 1985; Yates et al. 1985) and recovery time (Rhode and Smith 1986). Across different fibers, the ratio varies with SR and CF (Rhode and Smith 1986).

Adaptation studies of AN fibers have demonstrated that more than one form of adaptation must exist (Chimento and Schreiner 1991; Furukawa and Matsuura 1978; Westerman and Smith 1984, 1985; Yates et al. 1985), suggesting also that there may be more than one mechanism of adaptation (Yates et al. 1985). However, in contrast to some proposals (Chimento and Schreiner 1991), a tone burst of some fixed steady-state amplitude, but shaped with a rise function, does not provide a constant input to the system. Clearly, the input, as well as the IHC's receptor potential (Palmer and Russell 1986; Russell and Sellick 1983), is changing during the rise time. If the first spikes of an AN fiber, i.e., those that constitute the onset response component, are generated by the same mechanism as that proposed for AI neurons, then the effective stimulus for that onset component, viz. rate of change of peak pressure, is prevalent only during the rise time and is zero at its end. Thus the initial rapid adaptation of AN fibers to tone bursts, conventionally shaped with rise times of 1–5 ms, may be due to the cessation of the effective stimulus for the onset component after this brief period. The steady-state SPL reached at the end of the rise time then constitutes the effective stimulus for the sustained response. In this scenario, and ignoring short-term (Chimento and Schreiner 1991; Smith and Zwislocki 1975; Westerman and Smith 1984; Yates et al. 1985) and long-term adaptation (Javel 1996), there could be two different mechanisms leading to synaptic transmitter release from the hair cell and to spike generation in the afferent fiber. One mechanism gives rise to the steady-state discharge rate. In this case, synaptic transmission depends on the magnitude of the receptor potential, and it might be mediated by voltage-gated Ca^{2+} channels that inactivate little (steady-state Ca^{2+} conductances). The other mechanism gives rise to the onset response. Here, synaptic transmission depends on a *change* of the receptor potential, and it might be mediated by rapidly inactivating Ca^{2+} conductances. Vertebrate hair cells appear to be equipped with voltage-gated Ca^{2+} channels that are distinctly different from those of most central neurons (for reviews see Dunlap et al. 1995; Fuchs 1996). Voltage-gated Ca^{2+} channels of hair cells hitherto identified are dihydropyridine sensitive and noninactivating, possibly related to the neuronal L-type channels, and they seem ideally suited to mediate steady-state discharge rates. There is evidence that hair cells can express more than one type of voltage-gated Ca^{2+} channel (e.g., Su et al. 1995). Rapidly inactivating T-type Ca^{2+} channels have not yet been identified in vertebrate hair cells, possibly due to the lack of selective antagonists (Dunlap et al. 1995), but transient T-type Ca^{2+} *currents* have been recorded in guinea pig vestibular hair cells (Rennie and Ashmore 1991). These authors observed that the rate of rise of the transient Ca^{2+} currents and the time-to-peak varied with the magnitude of the steplike depolarization. Furthermore, the maximum size of the current varied widely among different hair cells. Given these findings, it is conceivable that, in IHCs of the mammalian cochlea, noninactivating and rapidly inactivating voltage-gated Ca^{2+} channels may coexist, with different ratios at different synapses of the same hair cell and across different hair cells.

Origin of the latency-acceleration function

The fact that AN and AI latency is an invariant function of maximum acceleration of peak pressure does not mean that it is the time of occurrence of this stimulus feature that determines latency. For example, it is evident from the bottom row of Fig. 1 that for signals with a common maximum acceleration of peak pressure, the initial time course of the peak pressure (and that of the rate of change of peak pressure) is also very similar. It might therefore be argued that the critical variable in determining latency is not APP_{max} but the fact that the different signals all reach some particularly low (''threshold'') peak pressure at nearly the same instant. However, as inferred from the detailed analysis of the latency behavior of AI neurons (Heil 1997a,b; Heil and Irvine 1996), this is likely not the case. In response to signals of the same maximum acceleration of peak pressure, the first spike of AI neurons can be triggered at quite different signal amplitudes (see Fig. 8 in Heil 1997b). Furthermore, careful analysis of responses to linear rise function tones showed

that the change in an AI neuron's latency with alterations of the rise time and the plateau peak pressure (both affecting the rate of change of peak pressure) is incompatible with such a firing threshold interpretation of latency and the opposite of what would be expected if adaptive processes or accommodation were to prolong the time necessary to reach the presumed threshold for long rise times or low rates of change of peak pressure (Heil and Irvine 1996). Because latency-acceleration functions of AN fibers are very similar to those of AI neurons (see Fig. 6), the threshold model is probably also inadequate to explain the latency behavior of AN fibers. However, the unequivocal verification of this hypothesis requires knowledge of the true response latencies of AN fibers, knowledge that cannot be obtained due to the fibers' spontaneous activity.

Despite this qualification, the data of the present study support our previous conclusion (Heil 1997a) that the characteristics of the latency-acceleration functions of AI neurons reflect processes at the synapses between IHCs and AN fibers. We would like to tentatively propose here that the system, consisting of an IHC and its synapse with a particular afferent fiber, determines the *shape* of the latency-acceleration function. The traveling wave imposes a CF-dependent delay, and the same factors that determine the hearing sensitivity of the animal, viz. structures of the outer, middle, and inner ears, impose a CF-dependent horizontal dispersion on the latency-acceleration functions, i.e., differences in transient sensitivity. Thus, when the latency-acceleration functions are corrected for these differences and for the differences in cochlear travel delays, any IHC–afferent fiber system would act in much the same fashion with respect to the transduction of acceleration of peak pressure into the first-spike latency. Some differences in latency characteristics among the afferent fibers innervating a single IHC will remain after such corrective procedures. These are differences in minimum latency and in transient sensitivity, although the latter differences are smaller than suggested by the vertical scatter of S estimates at a given CF in Fig. 8, which reflects, at least in part, the effect of SR on S etimates as outlined above. These differences would have to be attributed to differences in synaptic morphology or in afferent fiber properties (Merchan-Perez and Liberman 1996). On this view, the stimulus-dependent component of the standard deviation, viz. $(k * \dot{L})$ (see *Eqs. 8* and *9*) would also have its origin in trial-to-trial fluctuations of the acceleration of peak pressure, as sensed by the hair cell, thus basically in jitter of cochlear mechanics and transduction mechanisms.

The implications of the data for cochlear transduction processes are also of interest. Our data show that the latency of AN fiber responses at high frequencies (note that the vast majority of our data were obtained above 3 kHz and the lowest CF was 600 Hz) is a function of the maximum acceleration of peak pressure. This characteristic of the stimulus envelope is presumably reflected in the DC receptor potential generated by an IHC, as at high frequencies that potential more or less closely follows the stimulus envelope (see, e.g., Fig. 2 in Russell and Sellick 1983). The results therefore imply that at these frequencies it may be the time of maximum acceleration of the DC receptor potential that determines the time at which transmitter is released and AN activity is evoked. Any extrapolation of our findings to lower frequencies must be speculative, and at least two possibilities need to be considered. At lower frequencies the time course of the envelope and that of the sound pressure itself become progressively more identical. Thus it may be that at low frequencies latency is a function of the acceleration of the sound pressure itself. Because the AC component, which dominates the IHC receptor potential at low frequencies, is approximately equal to the acceleration of the sound pressure, being maximal shortly after maximum acceleration toward rarefaction (Russell and Sellick 1983; see their Fig. 5), latency of the AN fiber may be a function of the AC amplitude. Alternatively, it might be the acceleration of the AC component that determines the time of AN activation; if so, that time would be a function of the fourth derivative of sound pressure, which for a sinusoid has the same time course as the sound pressure itself.

We are grateful to J. F. Cassell, V. N. Park, R. Williams, and other members of the general staff in the department for technical support; to distinguished colleagues who have contributed to our thinking about specific issues dealt with in the paper; and to Dr. A. R. Palmer and two anonymous reviewers for valuable comments on the manuscript.

This study was supported by the National Health and Medical Research Council of Australia.

Address reprint requests to P. Heil.

Received 24 December 1996; accepted in final form 1 July 1997.

REFERENCES

AITKIN, L. M. *The Auditory Cortex.* New York: Chapman and Hall, 1990.

ANDERSON, D. J., ROSE, J. E., HIND, J. E., AND BRUGGE, J. F. Temporal position of discharges in single auditory nerve fibers within the cycle of a sine-wave stimulus: frequency and intensity effects. *J. Acoust. Soc. Am.* 49: 1131–1139, 1971.

BRUGGE, J. F., DUBROVSKY, N. A., AITKIN, L. M., AND ANDERSON, D. J. Sensitivity of single neurons in in auditory cortex of cat to binaural tonal stimulation: effects of varying interaural time and intensity. *J. Neurophysiol.* 32: 1005–1024, 1969.

CALFORD, M. B. AND SEMPLE, M. N. Monaural inhibition in cat auditory cortex. *J. Neurophysiol.* 73: 1876–1891, 1995.

CARIANI, P. A. As if time really mattered: temporal strategies for neural coding of sensory information. *Commun. Cognit. Artif. Intell.* 12: 161–229, 1995.

CARIANI, P. A. AND DELGUTTE, B. Neural correlates of the pitch of complex tones. I. Pitch and pitch salience. *J. Neurophysiol.* 76: 1698–1716, 1996.

CHIMENTO, T. C. AND SCHREINER, C. E. Adaptation and recovery from adaptation in single fiber responses of the cat auditory nerve. *J. Acoust. Soc. Am.* 90: 263–273, 1991.

CLAREY, J. C., BARONE, P., AND IMIG, T. J. Physiology of thalamus and cortex. In: *The Mammalian Auditory Pathway: Neurophysiology,* edited by A. N. Popper and R. R. Fay. New York: Springer-Verlag, 1992, p. 232–334.

DUNLAP, K., LUEBKE, J. I., AND TURNER, T. J. Exocytotic Ca^{2+} in mammalian central neurons. *Trends Neurosci.* 18: 89–98, 1995.

EGGERMONT, J. J. Rate and synchronization measures of periodicity coding in cat primary auditory cortex. *Hear. Res.* 56: 153–167, 1991.

EVANS, E. F. AND WHITFIELD, I. C. Classification of unit responses in the auditory cortex of the unanesthetized and unrestrained cat. *J. Physiol. (Lond.)* 171: 476–493, 1964.

FERSTER, D. AND SPRUSTON, N. Cracking the neural code. *Science* 270: 756–758, 1995.

FUCHS, P. A. Synaptic transmission at vertebrate hair cells. *Curr. Opin. Neurobiol.* 6: 514–519, 1996.

FURUKAWA, T. AND MATSUURA, S. Adaptive rundown of excitatory postsynaptic potentials at synapses between hair cells and eighth nerve fibres in the goldfish. *J. Physiol. (Lond.)* 276: 193–209, 1978.

GOLDSTEIN, J. L., BAER, T., AND KIANG, N.Y.S. A theoretical treatment of

latency, group delay, and tuning characteristics for auditory-nerve responses to clicks and tones. In: *Physiology of the Auditory System*, edited M. B. Sachs. Baltimore, MD: National Academy Consultants, 1971, p. 241–248.

HEIL, P. Auditory onset responses revisited. I. First-spike timing. *J. Neurophysiol.* 77: 2616–2641, 1997a.

HEIL, P. Auditory onset responses revisited. II. Response strength. *J. Neurophysiol.* 77: 2642–2660, 1997b.

HEIL, P. AND IRVINE, D.R.F. On determinants of first-spike latency in auditory cortex. *Neuroreport* 7: 3073–3076, 1996.

HEIL, P., RAJAN, R., AND IRVINE, D.R.F. Sensitivity of neurons in cat primary auditory cortex to tones and frequency-modulated stimuli. I. Effects of variation of stimulus parameters. *Hear. Res.* 63: 108–134, 1992a.

HEIL, P., RAJAN, R., AND IRVINE, D.R.F. Sensitivity of neurons in cat primary auditory cortex to tones and frequency-modulated stimuli. II. Organization of response properties along the ''isofrequency'' dimension. *Hear. Res.* 63: 135–156, 1992b.

HEIL, P., RAJAN, R., AND IRVINE, D. R. F. Topographic representation of tone intensity along the isofrequency axis of cat primary auditory cortex. *Hearing Res.* 76: 188–202, 1994.

HEIL, P. AND SCHEICH, H. Functional organization of the avian auditory cortex analogue. II. Topographic distribution of latency. *Brain Res.* 539: 121–125, 1991.

HEIL, P., SCHULZE, H., AND LANGNER, G. Ontogenetic development of periodicity coding in the inferior colliculus of the mongolian gerbil. *Auditory Neurosci.* 1: 363–383, 1995.

HOPFIELD, J. J. Pattern recognition computation using action potential timing for stimulus representation. *Nature* 376: 33–36, 1995.

IRVINE, D.R.F. Physiology of the auditory brainstem. In: *The Mammalian Auditory Pathway: Neurophysiology*, edited by A. N. Popper and R. R. Fay. New York: Springer-Verlag, 1992, p. 153–231.

JAVEL, E. Long-term adaptation in cat auditory-nerve fiber responses. *J. Acoust. Soc. Am.* 99: 1040–1052, 1996.

JORIS, P. X., CARNEY, L. H., SMITH, P. H., AND YIN, T.C.T. Enhancement of neural synchronization in the anteroventral cochlear nucleus. I. Responses to tones at the characteristic frequency. *J. Neurophysiol.* 71: 1022–1036, 1994.

JORIS, P. X. AND YIN, T.C.T. Responses of amplitude-modulated tones in the auditory nerve of the cat. *J. Acoust. Soc. Am.* 91: 215–232, 1992.

KIANG, N.Y.-S., WATANABE, T., THOMAS, E. C., AND CLARK, L. F. Discharge patterns of single fibers in the cat's auditory nerve. *MIT Research Monograph* 35: 1965.

KIM, D. O. AND MOLNAR, C. E. A population study of cochlear nerve fibres: comparison of spatial distributions of average rate and phase-locking measures of responses to single tones. *J. Neurophysiol.* 42: 16–30, 1979.

KITZES, L. M., GIBSON, M. M., ROSE, J. E., AND HIND, J. E. Initial discharge latency and threshold considerations for some neurons in cochlear nucleus complex of the cat. *J. Neurophysiol.* 41: 1165–1182, 1978.

KÖNIG, P., ENGEL, A. K., AND SINGER, W. Integrator or coincidence detector? The role of the cortical neuron revisited. *Trends Neurosci.* 19: 130–137, 1996.

LANGNER, G., SCHREINER, C. E., AND MERZENICH, M. M. Covariation of response latency and temporal resolution in the inferior colliculus of the cat. *Hear. Res.* 31: 197–202, 1987.

LIBERMAN, M. C. Auditory nerve responses from cats raised in a low noise chamber. *J. Acoust. Soc. Am.* 63: 442–455, 1978.

LIBERMAN, M. C. Morphological differences among radial afferent fibers in the cat cochlea: an electron-microscopic study of serial sections. *Hear. Res.* 3: 45–63, 1980.

LIBERMAN, M. C. Single-neuron labeling in the cat auditory nerve. *Science* 216: 1239–1241, 1982.

LIBERMAN, M. C. Physiology of cochlear efferent and afferent neurons: direct comparison in the same animal. *Hear. Res.* 34: 179–192, 1988.

LIBERMAN, M. C. AND BROWN, M. C. Physiology and anatomy of single olivocochlear neurons in the cat. *Hear. Res.* 24: 17–36, 1986.

MERCHAN-PEREZ, A. AND LIBERMAN, M. C. Ultrastructural differences among afferent synapses on cochlear hair cells: correlations with spontaneous discharge rate. *J. Comp. Neurol.* 371: 208–221, 1996.

MIDDLEBROOKS, J. C., CLOCK, A. E., XU, L., AND GREEN, D. M. A panoramic code for sound location by cortical neurons. *Science* 264: 842–844, 1994.

PALMER, A. R. AND RUSSELL, I. J. Phase-locking in the cochlear nerve of the guinea-pig and its relation to the receptor potential of inner hair-cells. *Hear. Res.* 24: 1–13, 1986.

PHILLIPS, D. P. Neural representation of sound amplitude in the auditory cortex: effects of noise masking. *Behav. Brain Res.* 37: 197–214, 1990.

PHILLIPS, D. P. Neural representation of stimulus times in the primary auditory cortex. *Ann. NY Acad. Sci.* 682: 104–118, 1993.

PHILLIPS, D. P. AND HALL, S. E. Response timing constraints on the cortical representation of sound time structure. *J. Acoust. Soc. Am.* 88: 1403–1411, 1990.

PHILLIPS, D. P., KITZES, L. M., SEMPLE, M. N., AND HALL, S. E. Stimulus-induced spike bursts in two fields of cat auditory cortex. *Hear. Res.* 97: 165–173, 1996.

PHILLIPS, D. P. AND SARK, S. A. Separate mechanisms control spike numbers and inter-spike intervals in transient responses of cat auditory cortex neurons. *Hear. Res.* 53: 17–27, 1991.

PHILLIPS, D. P., SEMPLE, M. N., AND KITZES, L. M. Factors shaping the tone level sensitivity of single neurons in posterior field of cat auditory cortex. *J. Neurophysiol.* 73: 674–686, 1995.

RAJAN, R., IRVINE, D.R.F., AND CASSELL, J. F. Normative N1 audiogram data for the barbiturate-anesthetized domestic cat. *Hear. Res.* 53: 153–158, 1991.

RENNIE, K. J. AND ASHMORE, J. F. Ionic currents in isolated vestibular hair cells from the guinea-pig crista ampullaris. *Hear. Res.* 51: 279–292, 1991.

RHODE, W. S. AND GREENBERG, S. Physiology of the cochlear nuclei. In: *The Mammalian Auditory Pathway: Neurophysiology*, edited by A. N. Popper and R. R. Fay. New York: Springer-Verlag, 1992, p. 94–152.

RHODE, W. S. AND SMITH, P. H. Characteristics of tone-pip response patterns in relationship to spontaneous rate in cat auditory nerve fibers. *Hear. Res.* 18: 159–168, 1985.

RHODE, W. S. AND SMITH, P. H. Encoding timing and intensity in the ventral cochlear nucleus of the cat. *J. Neurophysiol.* 56: 261–268, 1986.

RUGGERO, M. A. Physiology and coding of sound in the auditory nerve. In: *The Mammalian Auditory Pathway: Neurophysiology*, edited by A. N. Popper and R. R. Fay. New York: Springer-Verlag, 1992, p. 34–93.

RUGGERO, M. A. AND RICH, N. C. Timing of spike initiation in cochlear afferents in cochlear afferents: dependence on site of innervation. *J. Neurophysiol.* 58: 379–403, 1987.

RUSSELL, I. J. AND SELLICK, P. M. Low-frequency characteristics of intracellularly recorded receptor potentials in guinea-pig cochlear hair cells. *J. Physiol. (Lond.)* 338: 179–206, 1983.

SACHS, M. B. AND ABBAS, P. J. Rate versus level fucntions for auditory nerve fibers in cats: tone burst stimulation. *J. Acoust. Soc. Am.* 56: 1835–1847, 1974.

SCHREINER, C. E., MENDELSON, J. R., AND SUTTER, M. L. Functional topography of cat primary auditory cortex: representation of tone intensity. *Exp. Brain Res.* 92: 105–122, 1992.

SCHREINER, C. E. AND URBAS, J. V. Representation of amplitude modulation in the auditory cortex of the cat. II. Comparison between cortical fields. *Hear. Res.* 32: 49–64, 1988.

SMITH, R. L. AND ZWISLOCKI, J. J. Short-term adaptation and incremental responses of single auditory-nerve fibers. *Biol. Cybern.* 17: 169–182, 1975.

SOKOLICH, W. G. Closed sound delivery systems. United States Patent 4251686, 1981.

SU, Z.-L., JIANG, S.-C., GU, R., AND YANG, W.-P. Two types of calcium channels in bullfrog saccular hair cells. *Hear. Res.* 87: 62–68, 1995.

VIEMEISTER, N. F. AND PLACK, C. J. Time analysis. In: *Human Psychophysics*, edited by W. A. Yost, A. N. Popper, and R. R. Fay. New York: Springer-Verlag, 1993, p. 116–154.

WESTERMAN, L. A. AND SMITH, R. L. Rapid and short-term adaptation in auditory nerve responses. *Hear. Res.* 15: 249–260, 1984.

WESTERMAN, L. A. AND SMITH, R. L. Rapid adaptation depends on the characteristic frequency of auditory nerve fibers. *Hear. Res.* 17: 197–198, 1985.

WINTER, I. M., ROBERTSON, D., AND YATES, G. K. Diversity of characteristic frequency rate-intensity functions in guinea pig auditory nerve fibres. *Hear. Res.* 45: 191–202, 1990.

YATES, G. K., ROBERTSON, D., AND JOHNSTONE, B. M. Very rapid adaptation in the guinea pig auditory nerve. *Hear. Res.* 17: 1–12, 1985.